OPEN ACCESS

Original research

PD-L1 blockade liberates intrinsic antitumourigenic properties of glycolytic macrophages in hepatocellular carcinoma

Li-Gong Lu,[1] Zhi-Ling Zhou,[1] Xu-Yan Wang,[1] Bo-Yuan Liu,[2,3] Jin-Ying Lu,[2,3] Shuai Liu,[2,3] Guang-Bo Zhang,[4] Mei-Xiao Zhan,[1] Yun Chen [2,3]

► Additional supplemental material is published online only. To view, please visit the journal online (http://dx.doi.org/10.1136/gutjnl-2021-326350).

For numbered affiliations see end of article.

Correspondence to
Dr Yun Chen, Nanjing Medical University, Nanjing, China; chenyun@njmu.edu.cn, Dr Mei-Xiao Zhan and Dr Li-Gong Lu, Zhuhai People's Hospital, Zhuhai, China; zhanmeixiao1987@126.com, luligong1969@jnu.edu.cn and Dr Guang-Bo Zhang, The First Affiliated Hospital of Soochow University, Suzhou, China; zhanggbsuzhou@hotmail.com

L-GL, Z-LZ and X-YW are joint first authors.
LL, G-BZ, MZ and YC are joint senior authors.

Received 18 October 2021
Accepted 6 February 2022
Published Online First 16 February 2022

To cite: Lu L-G, Zhou Z-L, Wang X-Y, *et al*. *Gut* 2022;**71**:2551–2560.

ABSTRACT

Objective Patients with increased PD-L1$^+$ host cells in tumours are more potent to benefit from antiprogrammed death-1/programmed death ligand-1 (PD-L1) treatment, but the underlying mechanism is still unclear. We aim to elucidate the nature, regulation and functional relevance of PD-L1$^+$ host cells in hepatocellular carcinoma (HCC).

Design A total of untreated 184 HCC patients was enrolled randomly. C57BL/6 mice are given injection of Hepa1-6 cells to form autologous hepatoma. ELISpot, flow cytometry and real-time PCR are applied to analyse the phenotypic characteristics of PD-L1$^+$ cells isolated directly from HCC specimens paired with blood samples or generated from ex vivo and in vitro culture systems. Immunofluorescence and immunohistochemistry are performed to detect the presence of immune cells on paraffin-embedded and formalin-fixed samples. The underlying regulatory mechanisms of metabolic switching are assessed by both in vitro and in vivo studies.

Results We demonstrate that PD-L1$^+$ host macrophages, which constructively represent the major cellular source of PD-L1 in HCC tumours, display an HLA-DR^{high}CD86^{high} glycolytic phenotype, significantly produce antitumourigenic IL-12p70 and are polarised by intrinsic glycolytic metabolism. Mechanistically, a key glycolytic enzyme PKM2 triggered by hepatoma cell derived fibronectin 1, via a HIF-1α-dependent manner, concurrently controls the antitumourigenic properties and inflammation-mediated PD-L1 expression in glycolytic macrophages. Importantly, although increased PKM2$^+$ glycolytic macrophages predict poor prognosis of patients, blocking PD-L1 on these cells eliminates PD-L1-dominant immunosuppression and liberates intrinsic antitumourigenic properties.

Conclusions Selectively modulating the 'context' of glycolytic macrophages in HCC tumours might restore their antitumourigenic properties and provide a precise strategy for anticancer therapy.

Significance of this study

What is already known on this subject?

⇒ Hepatocellular carcinoma (HCC) is the fifth most common cancer worldwide, with an extremely poor prognosis.
⇒ Patients with increased PD-L1$^+$ host cells in tumours are more potent to benefit from antiprogrammed death-1/programmed death ligand-1 (PD-L1) treatment.
⇒ Macrophages constitute a major component of the leucocyte infiltrate in hepatocellular carcinoma (HCC) tumour stroma.
⇒ Macrophage polarisation is closely linked to changes in the cellular metabolic programmes.

What are the new findings?

⇒ PD-L1$^+$ host macrophages display an HLA-DR^{high}CD86^{high} phenotype and significantly produce antitumourigenic IL-12p70 in HCC.
⇒ Intrinsic glycolytic metabolism shapes PD-L1$^+$ macrophages with antitumourigenic properties in HCC.
⇒ PKM2/HIF-1α axis, elicited by hepatoma cell-derived fibronectin 1, triggers pluripotent polarisation of macrophages.
⇒ PD-L1 blockade eliminates PD-L1-dominant immunosuppression and liberates intrinsic antitumour capability of glycolytic macrophages.

How might it impact on clinical practice in the foreseeable future?

⇒ Increased PKM2$^+$ glycolytic macrophages predict poor prognosis of patients, blocking PD-L1 on those cells liberates intrinsic antitumourigenic activties.
⇒ Selectively modulating the 'context' of glycolytic macrophages in HCC tumours might provide a precise strategy for anticancer therapy.

INTRODUCTION

Programmed death ligand-1 (PD-L1) is a promising therapeutic target in aggressive cancers.[1–4] PD-L1 is chiefly detected in inflamed epithelial tissues, cancer cells or host stromal cells; its expression is assumed as a predictive biomarker of benefit from anti-PD-1/PD-L1 treatment.[5–7] However, several clinical studies have emphasised that patients with increased PD-L1$^+$ host cells are more likely to benefit from anti-PD-1/PD-L1 treatment than those with increased PD-L1$^+$ cancer cells.[8–10] At present, the nature, regulation and functions of PD-L1$^+$ host cells in human cancers are indeed unclear.

Macrophages constitute a major component of the leucocyte infiltrate in tumour stroma.[11] In response to environmental signals, these cells acquire special phenotypic characteristics that are associated with diverse functions.[12 13] It is worth noting that polarisation of macrophages is closely related to the changes of cellular metabolic programme.[14 15] In both mice and humans, glycolytic metabolism is involved in classical activation of macrophages (M1), whereas mitochondrial oxidative phosphorylation (OXPHOS) is restricted to alternative activation of macrophages (M2).[16] Up until now, little is known about whether and how metabolic changes might occur and regulate the phenotypes and functions of macrophages in a tumour environment.

Hepatocellular carcinoma (HCC) is the fifth most common cancer worldwide, with an extremely poor prognosis.[17 18] By using HCC as a model system, the present study shows that PD-L1$^+$ host macrophages, which constructively represent the major cellular source of PD-L1 in HCC tumours, display an HLA-DR^{high}CD86^{high} glycolytic phenotype, significantly produce antitumourigenic IL-12p70 and are polarised by intrinsic glycolytic metabolism. Mechanistically, a key glycolytic enzyme PKM2 triggered by hepatoma cell-derived fibronectin 1 (FN1), via a HIF-1α-dependent manner, concurrently controls the antitumourigenic properties and inflammation-mediated PD-L1 expression in glycolytic macrophages. More importantly, although increased PKM2$^+$ glycolytic macrophages predict poor prognosis of patients, blocking PD-L1 on these cells eliminates PD-L1-dominant immunosuppression and liberates intrinsic antitumourigenic properties.

MATERIALS AND METHODS

Patients and specimens

Tissues and paired blood samples were obtained from patients who underwent curative resection at the First Affiliated Hospital of Nanjing Medical University (online supplemental table 1). None of the patients had received anticancer therapy before sampling, and those with concurrent autoimmune disease, HIV or syphilis were excluded. Ninety-one patients who had complete follow-up data were used for immunohistochemistry and immunofluorescence analysis and/or assessments of disease-free survival (cohort 1; online supplemental table 1). Paired fresh samples of blood and tumour tissues from 93 HCC patients who underwent surgical resection between December 2018 and December 2021 were used for isolating peripheral and tissue-infiltrating leukocytes (cohort 2; online supplemental table 1). Clinical stages were classified according to the guidelines of the International Union Against Cancer.

Animals, cell lines, reagents and primers

Wild-type C57BL/6J mice (6–8 weeks old, female) were purchased from the Nanjing Biomedical Research Institute of Nanjing University. Human Liver cell (L02), HEK293T and Huh7 cell lines were obtained from the American Type Culture Collection. The antibodies used in fluorescence-activated cell sorting/analyses are shown in online supplemental table 2. The antibodies used in immunoblotting and immunohistochemistry/immunofluorescence are shown in online supplemental table 3. The primers used in real-time PCR are listed in online supplemental table 4, and all other reagents are summarised in online supplemental table 5 unless indicated in the text.

Statistical analysis

Results are presented as mean±SEM. No data have been excluded. All statistical tests were performed as two sided. For data normally distributed, we applied the Student's t-test, and the non-parametric exact Wilcoxon signed-rank test was used to compare data not normally distributed. For multiple comparisons, an analysis of variance followed by Bonferroni's correction was applied. R values were calculated based on the analysis of Pearson's correlation. All statistical tests were performed with GraphPad Prism (V.6) software. Differences with $p<0.05$ were considered statistically significant.

Additional methods

Other methods are detailed in online supplementary materials and methods.

RESULTS

Intrinsic glycolytic metabolism polarises PD-L1$^+$ macrophages in human hepatoma

We used confocal microscopy to examine the expression pattern of PD-L1 in HCC specimens (n=10) and found that PD-L1 was expressed mainly by CD68$^+$ macrophages and was only weakly expressed by other stromal and hepatoma cells (figure 1A). To further confirm the source of PD-L1, we prepared single cell suspensions from HCC tumour and paired non-tumoural liver and blood (n=9; online supplemental figure 1A,B). PD-L1 was weakly expressed on blood monocytes (figure 1B). Although the percentage of PD-L1$^+$ macrophages (CD14$^{+/dim}$ cells) was also increased in peritumoural liver tissues, the intensity of PD-L1 expression was low (figure 1B). As expected, most tumour tissues contained a significantly greater proportion of PD-L1$^{+/high}$ macrophages (figure 1B). In contrast, PD-L1 was hardly or only weakly expressed by other stromal cells, including B cells, T cells, NK cells and neutrophils, as well as CD45$^-$ non-haematopoietic cells in HCC tumours (online supplemental figure 1C,D). Thus, host macrophages are major sources of PD-L1 in HCC tumours.

It is noteworthy that macrophage polarisation is closely linked to changes in the cellular metabolic programmes.[14–16] To examine whether metabolic process determined macrophage PD-L1 expression, we applied real-time PCR to compare the transcriptional profiles of metabolic enzymes in PD-L1$^+$ and PD-L1$^-$ macrophages from HCC tumours (n=3; online supplemental figure 1E). In general, PD-L1$^-$ macrophages chiefly expressed metabolic enzymes related to mitochondrial OXPHOS (figure 1C), revealing a metabolic quiescent state. Interestingly, PD-L1$^+$ macrophages markedly expressed the key rate-limiting glycolytic enzymes (figure 1C,D and online supplemental figure 1F). We evaluated the extracellular acidification rate, which quantifies proton production as a surrogate for lactate production and thus reflects overall glycolytic flux.[19] In support, PD-L1$^+$ macrophages exhibited substantially higher basal and maximal glycolytic rates compared with PD-L1$^-$ macrophages (figure 1E). We also detected an obvious upregulation of glucose transporter Glut1 in PD-L1$^+$ macrophages (figure 1F), suggesting an enhancement of glucose incorporation. Accordingly, PD-L1$^+$ macrophages cultured ex vivo displayed a greater capacity to incorporate the fluorescent glucose analogue 2-(N-[7-nitrobenz-2-oxa-1,3-diazol-4-yl] amino)-2-deoxyglucose (2-NBDG) (figure 1G) and produced significantly more lactate (figure 1H).

The results described previously suggested that glycolytic metabolism may be involved in PD-L1 upregulation on tumour macrophages. To test this, we used specific inhibitors to reprogramme the metabolic processes of macrophages isolated from human HCC tumours ex vivo. Consistent with our hypothesis, a significant decline of PD-L1 expression in macrophages after exposing to 2-deoxyglucose (2-DG), a

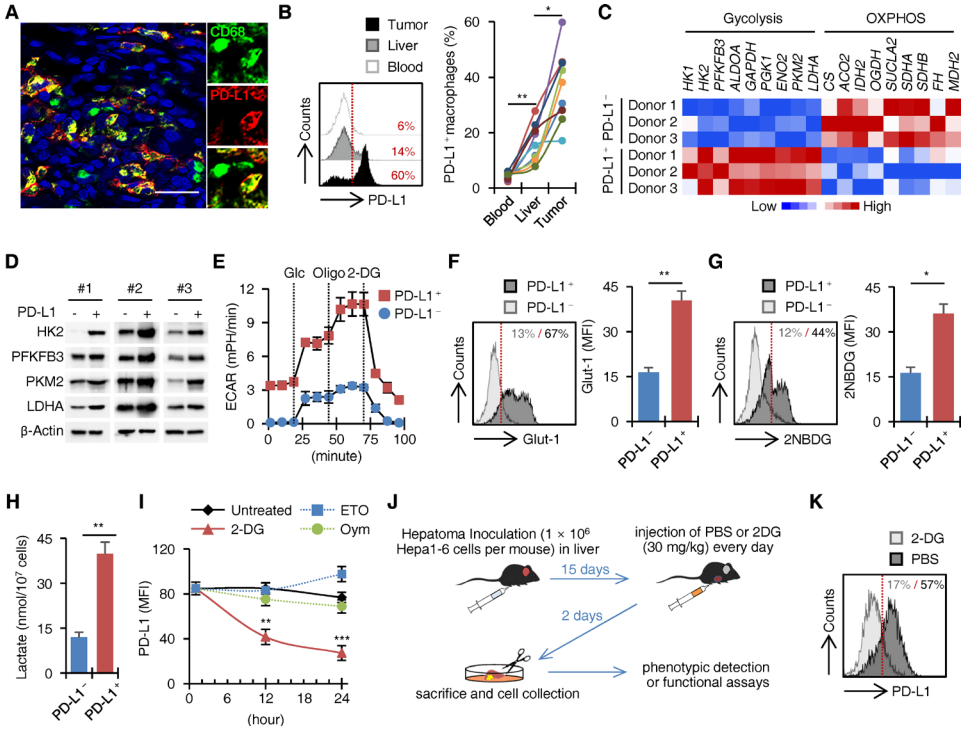

Figure 1 Glycolysis triggers PD-L1 on macrophages in human HCC tumours. (A) Confocal microscopy analysis of CD68$^+$PD-L1$^+$ cells in HCC tumours (n=10). Scale bar=100 µm. (B) FACS analysis of PD-L1 on monocytes/macrophages from HCC samples paired with blood samples (n=9). (C–H) Analysis of metabolic gene expression (C and D, n=3 for each), extracellular acidification rate (ECAR) (E, n=4), GLUT-1 expression (F, n=5), 2NBDG incorporation (G, n=5) and 20-hour lactate production (H, n=6) in PD-L1$^+$ and PD-L1$^-$ macrophages purified from human HCC tumours. (I) Effects of metabolic inhibitors 2-deoxyglucose (2-DG), etomoxir (ETO) and oligomycin (Oym) on ex vivo PD-L1 expression in macrophages from human HCC tumours (n=5). (J and K) Mice bearing Hepa1-6 hepatoma for 15 days were injected with PBS or 2-DG intraperitoneally as described (J). PD-L1 expression on tumour macrophages was determined by FACS (K, n=6). *P<0.05, **p<0.01, ***p<0.001. HCC, hepatocellular carcinoma; PD-L1, programmed death ligand-1.

glucose analogue that inhibits glucose incorporation, were observed (figure 1I). By comparison, PD-L1 expression was marginally affected by incubating macrophages with etomoxir (ETO), a widely used small-molecule inhibitor of fatty acid oxidation,[20] or with oligomycin, an inhibitor of ATP synthase (figure 1I).[21] Furthermore, the roles of glycolytic metabolism in PD-L1$^+$ macrophage induction were investigated in vivo (figure 1J). Consistently, intraperitoneal injection of 2-DG in Hepa1-6 hepatoma-bearing mice during the final 2 days of the experiment largely reduced the expression of PD-L1 in tumour macrophages (figure 1K).

PD-L1 blockade liberates antitumourigenic activity of glycolytic macrophages

We next asked whether inhibiting the glycolytic metabolism in tumour macrophages abrogated PD-L1-elicited immune privilege. To address that possibility, we purified PD-L1$^+$ and PD-L1$^-$ macrophages, as well as autologous infiltrating T cells from HCC tumour tissues, and then performed ELISpot assays (online supplemental figure 2A). Tumour T cells cocultured with the PD-L1$^+$ macrophages, but not the PD-L1$^-$ macrophages, exhibited an impaired production of IFN-γ (figure 2A). Consistent

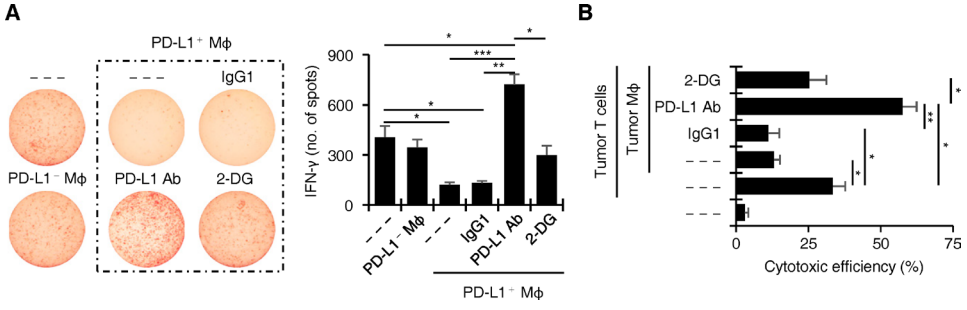

Figure 2 Glycolytic macrophages show intrinsic antitumourigenic properties. (A) IFN-γ detection by ELISpot in HCC tumour-derived T cells cultured alone or with PD-L1$^-$ or PD-L1$^+$ macrophages (Mϕ), or with those cells pre-treated with 2-DG, anti-PD-L1 antibody, or IgG1 as shown in online supplemental figure 2A (n=5). (B) cytotoxic effects of tumour T cells on CFSE-labelled autologous mouse Hepa1-6 hepatoma cells in the presence or absence of tumour Mϕ that were left untreated or pre-treated with 2-DG, anti-PD-L1 antibody, or IgG1 as shown in online supplemental figure 2B (n=6). propidium iodide$^+$ Hepa1-6 cells were measured by FACS. results are expressed as mean±SEM of three independent experiments. *p<0.05, **p<0.01, ***p<0.001.

with our hypothesis, suppressing the PD-L1 expression by pre-exposing PD-L1$^+$ macrophages to a glycolytic inhibitor 2-DG for 1 day (figure 1I) markedly restored the ability of tumour T cells to produce IFN-γ at levels comparable with that produced by untreated tumour T cells (figure 2A). Of note, we also blocked the PD-L1 by preincubation of PD-L1$^+$ macrophages with the monoclonal antibody (mAb) MIH1 in parallel. Remarkably, this treatment eliminated the immune privilege induced by macrophage PD-L1 and significantly and additionally enhanced the production of IFN-γ by T cells (figure 2A). Therefore, these data suggest that PD-L1$^+$ macrophages contain intrinsic antitumourigenic properties, which may be sustained by glycolytic metabolism but concealed by PD-L1 signals.

We afterward established an ex vivo autologous cytotoxic system using tumour-specific T cells derived from Hepa1-6 hepatoma-bearing mice (online supplemental figure 2B). As expected, tumour T cells cultured ex vivo effectively killed autologous Hepa1-6 cells, and this process was hampered by addition of autologous F4/80$^+$ tumour macrophages, but was further enhanced by adding those macrophages plus a specific antibody against murine PD-L1 (figure 2B). Supporting our hypothesis, tumour T cells cultured ex vivo with tumour macrophages that were pre-exposed to 2-DG only displayed the basal capabilities to kill autologous Hepa1-6 cells, but not an enhanced cytotoxic effect (figure 2B), suggesting that inhibition of glycolytic metabolism in macrophages also impairs their abilities to stimulate specific T cell response.

Glycolytic metabolism controls antitumourigenic properties and inflammation-elicited PD-L1 expression simultaneously in macrophages

Considering the intrinsic antitumourigenic properties of PD-L1$^+$ macrophages in human HCC (figure 2), we next probed the activation status and cytokine production profile of these cells. Interestingly, PD-L1$^+$ macrophages markedly expressed MHC class II molecule HLA-DR and costimulatory CD86, as compared with their PD-L1$^-$ counterparts (figure 3A); a marked

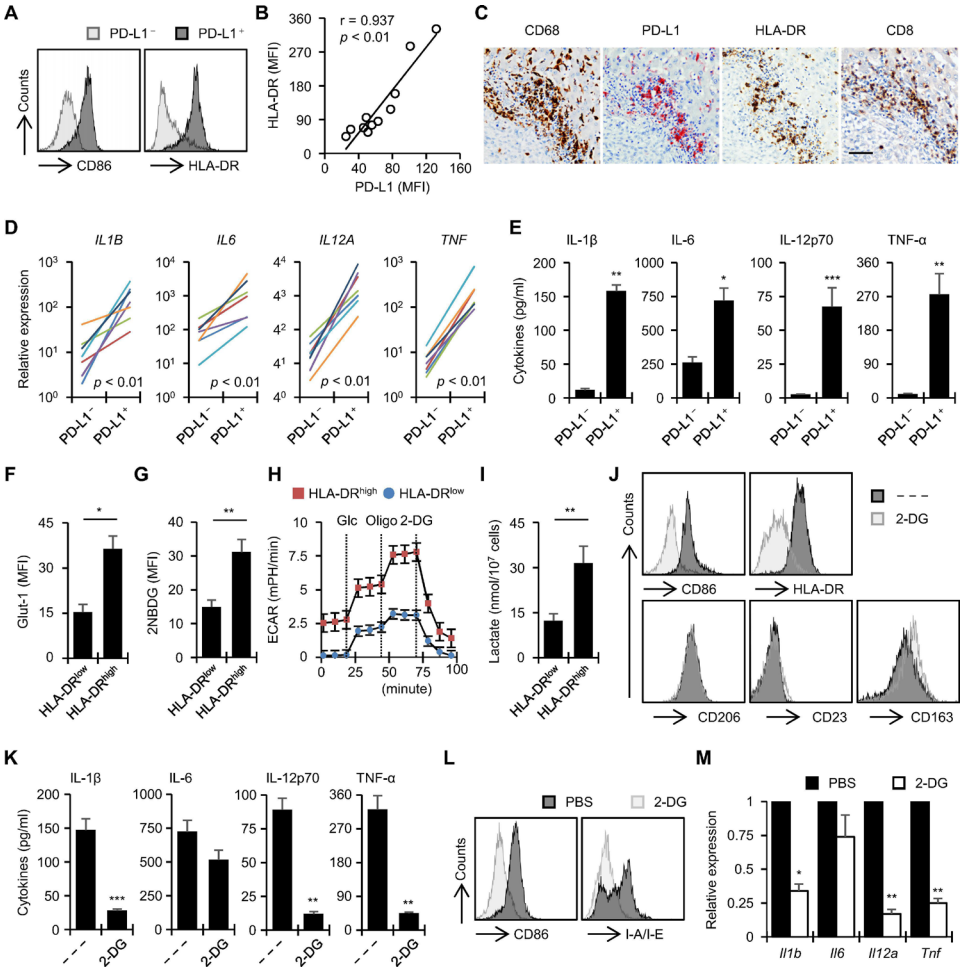

Figure 3 PD-L1$^+$ macrophages show a proinflammatory activated phenotype. (A) FACS analysis of CD86 and HLA-DR on PD-L1$^+$ and PD-L1$^-$ macrophages from HCC tumours (n=11). (B) Correlation between PD-L1 and HLA-DR expression in macrophages from human HCC tumours (n=11). (C) Immunohistochemistry analysis of CD68, PD-L1, HLA-DR and CD8 expression in HCC tumours (n=8). (D and E) Analysis of transcriptional and translational levels of IL-1β, IL-6, IL-12 and TNF-α in PD-L1$^+$ and PD-L1$^-$ macrophages from HCC tumours (n=7). (F–I) Analysis of glut-1 expression (F), 2NBDG incorporation (G), ECAR (H) and 20-hour lactate production (I) in HLA-DR^{high} and HLA-DR^{low} macrophages purified from human HCC tumours (n=5). (J and K) Effects of 2-DG on CD86, HLA-DR, CD206, CD23 and CD163 expression (J), as well as cytokine production (K), in macrophages from HCC tumours (n=4). (L and M) Mice (n=6) bearing Hepa1-6 hepatoma were injected with PBS or 2-DG as described in figure 1J. CD86 and I-A/I-E expression (L), as well as cytokine expression (M), in tumour macrophages were determined by FACS and real-time PCR, respectively. Results are expressed as mean±SEM of at least three independent experiments. *P<0.05, **p<0.01, ***p<0.001. 2-DG, 2-deoxyglucose; ECAR, extracellular acidification rate; HCC, hepatocellular carcinoma; PD-L1, programmed death ligand-1.

correlation between the intensities of PD-L1 and HLA-DR was detected in macrophages isolated from HCC tumours (n=11) (figure 3B). The coexistence of HLA-DR and PD-L1 on macrophages was further confirmed by examining expression of these proteins in serial sections of HCC tumour samples (n=8). Most of the HLA-DR^{high}PD-L1^{+} CD68 cells were accumulated in the invading edge, which also represented the main site of CD8^{+} cytotoxic T cells (figure 3C). In line with these findings, we further demonstrated that PD-L1^{+} tumour macrophages, but not their PD-L1^{-} counterparts, effectively expressed proinflammatory IL-1β, IL-6, and TNF-α, as well as the antitumourigenic IL-12p70 (figure 3D,E), a prominent inducer of Th1 responses in humans and in mice.[22 23] Correspondingly, we demonstrated that, although the anti-PD-L1 Ab additionally enhanced the production of IFN-γ by tumour T cells in an ELISpot detection system, this process could be significantly abolished by additional neutralisation of IL-12p70 (online supplemental figure 3A,B). Analogously, IL-12p70 alone markedly increased the production of IFN-γ by tumour T cells ex vivo, which was considerably attenuated by adding the PD-L1^{+} HEK293T transfectants, but not by the control transfectants (online supplemental figure 3C,D).

Given that glycolytic metabolism was crucial for PD-L1^{+} macrophage induction (figure 1), we assessed whether such a mechanism was also responsible for macrophage activation. In fact, HLA-DR^{high} macrophages from HCC tumour tissues were more potent in incorporating and utilising glucose (figure 3F,G), and these cells exhibited higher basal and maximal glycolytic rates and produced significantly more lactate, as compared with the HLA-DR$^{low/-}$ macrophages (figure 3H,I). Accordingly, inhibition of glycolytic metabolism in macrophages from HCC tumour tissues by 2-DG effectively impaired the expression of HLA-DR and CD86, as well as the production of IL-1β, IL-12p70 and TNF-α (figure 3J,K). In contrast, such a treatment hardly affected the expression of macrophage M2 makers CD23 and CD206 but weakly increased the expression of CD163 (figure 3J). Similar results were obtained in Hepa1-6 hepatoma-bearing mice: suppression of glycolytic metabolism by 2-DG during the final 2 days of the experiment markedly attenuated the expression of IA-IE, CD86 and inflammatory cytokines in tumour macrophages (figure 3L,M).

We then investigated whether PD-L1 expression and proinflammatory cytokine production in macrophages were interrelated. Indeed, blocking the PD-L1 by a mAb in PD-L1^{+} macrophages did not affect the production of IL-12p70, as well as proinflammatory IL-1β, IL-6 and TNF-α (online supplemental figure 4A). Inversely, expression of PD-L1 in tumour macrophages was inhibited 40%–50% by blocking IL-1β and TNF-α but was not reduced by blocking IL-6 or IL-12p70 (figure 4A and online supplemental figure 4B). Comparably, recombinant IL-1β effectively induced upregulation of PD-L1 on blood monocytes. Although recombinant TNF-α alone had a marginal effect, it did synergistically increase the IL-1β-mediated PD-L1 expression (figure 4B). These findings indicate that IL-1β signalling contributes to PD-L1 induction in activated macrophages dominantly, which is consistent with a recent observation in liver cancer.[24] Consistently, neutralisation of IL-1β plus TNF-α in Hepa1-6 hepatoma-bearing mice (figure 4C) successfully inhibited macrophage PD-L1 expression (figure 4D), suppressed tumour growth (figure 4E) and increased the infiltration of functional CD8^{+} T cells (figure 4F), but such treatment did not affect IL-12p70 expression (figure 4G). Therefore, glycolytic metabolism in macrophages simultaneously contributes to inflammation-mediated PD-L1 suppression and IL-12-dominant antitumourigenic activities.

Roles of hepatoma environments in glycolytic metabolism-elicited macrophage polarisation

To probe the mechanisms involved in glycolytic metabolism-elicited macrophage polarisation by a tumour environment, we first set out to establish conditions under which this process can be reliably reproduced in vitro. Human monocytes were incubated with supernatants from cultures of primary HCC cells (HCC-SN) or normal liver L02 cells (Liver-SN). Exposure to 20% HCC-SN, but not Liver-SN, for 24 hours did result in

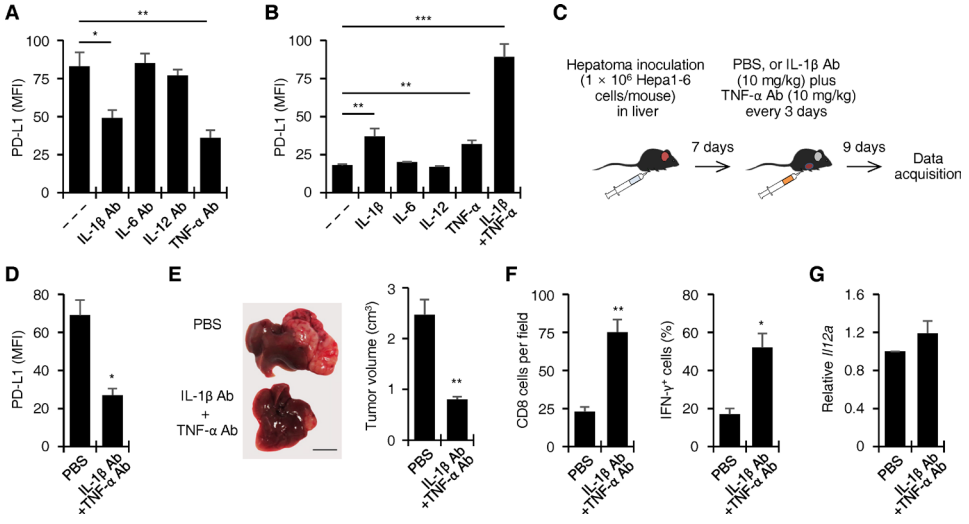

Figure 4 Inflammatory cytokines induce PD-L1 in tumour macrophages. (A) Twenty-four-hour blockade of IL-1β or TNF-α reduced PD-L1 expression in macrophages from human HCC tumours (n=5). (B) Exposure of blood CD14^{+} cells to IL-1β and/or TNF-α for 24 hours led to PD-L1 upregulation (n=5). (C–G) Mice bearing Hepa1-6 hepatoma were injected intraperitoneally with PBS or anti-IL-1β antibody plus anti-TNF-α antibody as shown (C, each n=6). Tumour macrophage PD-L1 expression (D), tumour size (E), CD8^{+} cell infiltration and function (F) and tumour macrophage *Il12a* expression (G) were determined. Results are expressed as mean±SEM of at least three independent experiments. *P<0.05, **p<0.01, ***p<0.001. HCC, hepatocellular carcinoma; PD-L1, programmed death ligand-1.

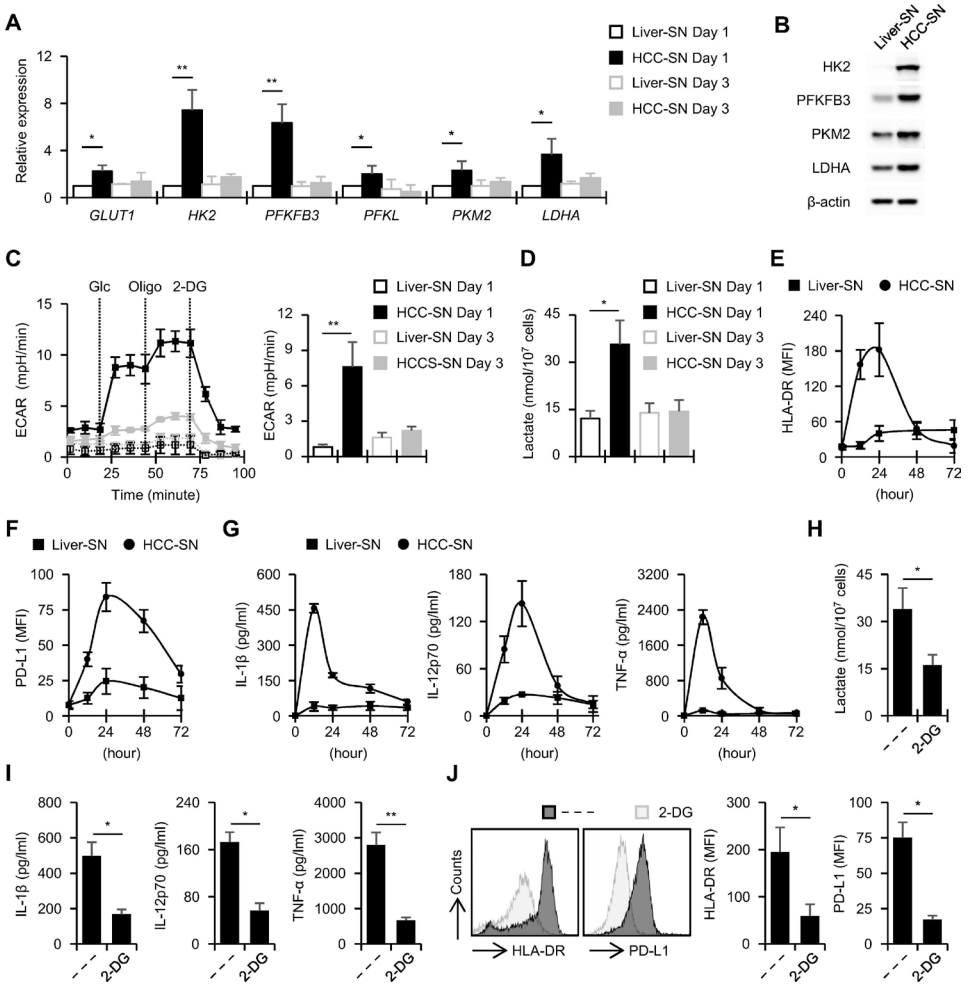

Figure 5 Hepatoma environments facilitate glycolysis and PD-L1 expression in macrophages. (A–G) Exposure of blood CD14$^+$ cells to primary HCC-SN, but not liver-SN, led to marked increases of glycolytic metabolic enzymes (A and B), ECAR (C), lactate production (D), HLA-DR expression (E), PD-L1 expression (F) and inflammatory cytokine production (G) after 24 hours but returned to a normal level after 3 days (n=7 for each). (H–J) Treatment of 2-DG for 24 hours suppressed HCC-SN-mediated upregulation of lactate production (H), inflammatory cytokine production (I) and HLA-DR and PD-L1 expression (J) in CD14$^+$ cells (n=7 for each). Results are expressed as mean±SEM of three independent experiments. *P<0.05, **p<0.01. 2-DG, 2-deoxyglucose; ECAR, extracellular acidification rate; HCC-SN, supernatants from cultures of primary HCC cells; PD-L1, programmed death ligand-1.

marked upregulation of the key rate-limiting glycolytic enzymes *GLUT1*, *HK2*, *PFKFB3*, *PFKL*, *PKM2* and *LDHA* in monocytes, but returned to a normal level after 3 days (figure 5A,B). Consistent with this, compared with the monocytes incubated with HCC-SN for 3 days, the cells exposing to HCC-SN for 24 hours displayed at least threefold higher maximal glycolytic rates and produced significantly more lactate (figure 5C,D). These data imply that active glycolytic metabolism mainly occurs in the early differentiation stage of macrophages in a tumour environment. In line with this, we observed that the expression of HLA-DR and PD-L1 was significantly upregulated on monocytes after their exposure to HCC-SN for 24 hours but was reduced on day 3 (figure 5E,F). Similar patterns of cytokine productions were obtained in HCC-SN-exposed monocytes, including the accumulations of proinflammatory IL-1β and TNF-α, as well as antitumourigenic IL-12p70, in the culture media at their early differentiation stage and a subsequent decline on day 3 (figure 5G). Furthermore, in support of conclusion mentioned previously that glycolytic metabolism-mediated proinflammatory response triggers PD-L1 expression in macrophages (figure 4), using a competitive inhibitor 2-DG to block the glycolytic metabolism of HCC-SN-exposed monocytes at their early differentiation stage (figure 5H) effectively impaired the production of IL-1β, IL-12p70 and TNF-α (figure 5I) and suppressed HLA-DR and PD-L1 expression (figure 5J).

PKM2/HIF-1α axis is crucial for pluripotent polarisation of macrophages in HCC

We further explored the signalling pathways involved in glycolytic metabolism-elicited macrophage polarisation. Considering the finding that the key rate-limiting glycolytic enzymes HK2, PFKFB3 and PKM2 were markedly elevated in HCC-SN-exposed monocytes (figure 5B), we used specific inhibitors to abolish the activities of these proteins during at their early differentiation stage (figure 6A and online supplemental figure 5). The results showed that suppressing PKM2 activity using ML-265 markedly reduced the production of IL-1β, IL-12p70 and TNF-α, as well as the expression of HLA-DR and PD-L1, by HCC-SN-exposed monocytes, although inhibiting the activity of HK2 by 3-BP or PFKFB3 by 3-PO marginally affected (figure 6B–D). We further used siRNA to confirm the roles of PKM2 proteins in regulating pluripotent polarisation of macrophages (figure 6E) and proved that this treatment effectively impaired the inflamed activities,

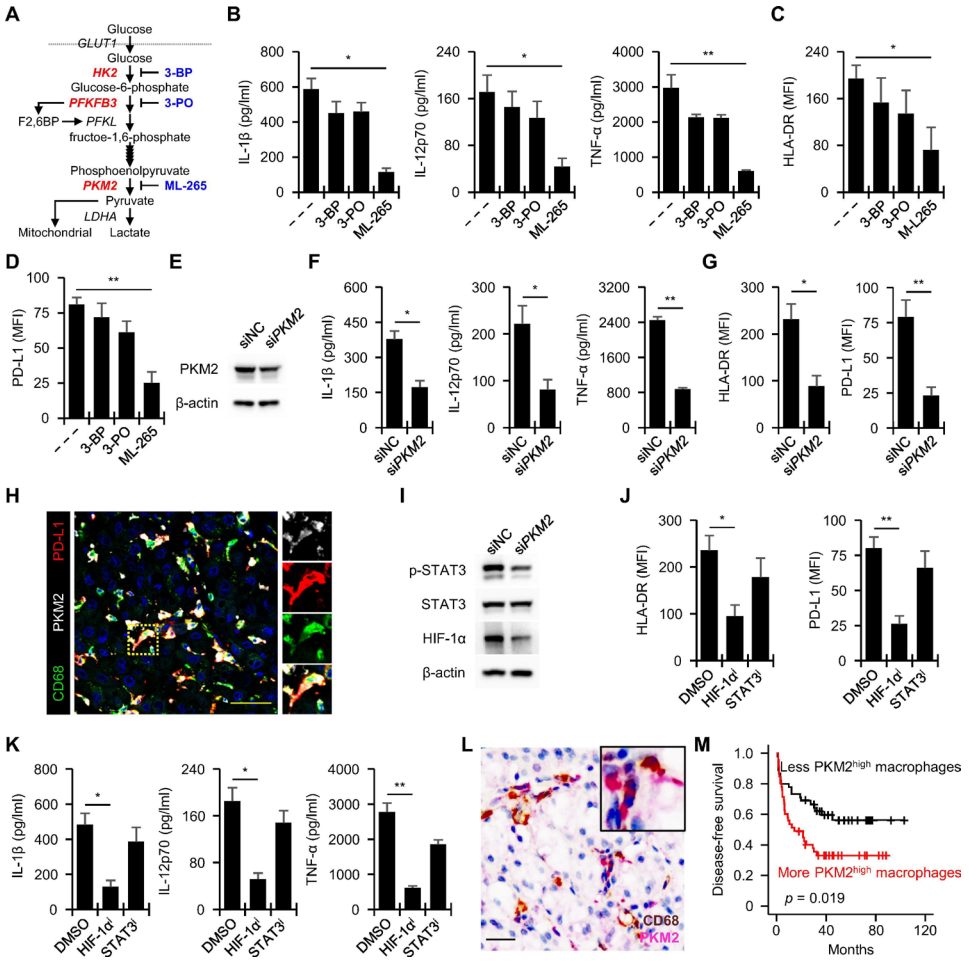

Figure 6 Glycolysis upregulates PD-L1 on macrophages via PKM2/HIF-1α axis-dependent manner. (A–D) Effects of 3-BP (an hK2 inhibitor), 3-PO (a PFKEB3 inhibitor) or ML-265 (a PKM2 inhibitor) (A) on inflammatory cytokine production (B), HLA-DR expression (C) and PD-L1 expression (D) by $CD14^+$ cells exposing to primary HCC-SN for 24 hours (n=5). (E–G) Transfection of si*PKM2* (E) suppressed cytokine production (F), as well as HLA-DR and PD-L1 expression (G), by $CD14^+$ cells exposing to primary HCC-SN for 24 hours (n=5). (H) Confocal microscopy analysis of CD68, PKM2 and PD-L1 distribution in HCC tumours (n=5). Scale bar=100 µm. (I) Transfection of si*PKM2* suppressed STAT3 activation and HIF-1α expression by $CD14^+$ cells exposing to primary HCC-SN (n=5). (J and K) Effects of STAT3 and HIF-1α inhibition on HLA-DR and PD-L1 expression (J), as well as inflammatory cytokine production (K), by $CD14^+$ cells exposing to primary HCC-SN for 24 hours (n=5). (L and M) Immunohistochemical analysis of $PKM2^+CD68^+$ cell distribution in HCC tumours (L, n=91). Patients were further divided into two groups according to the median value of the $PKM2^+CD68^+$ cell density in the tumour regions (less $PKM2^{high}$ macrophages, ≤90 cells (n=46); more $PKM2^{high}$ macrophages, >90 cells (n=45)). The disease-free survival rate of these patients was analysed with the Kaplan-Meier method and log-rank test (M). Scale bar=100 µm. Results are expressed as mean±SEM of at least four experiments. *P<0.05, **p<0.01. HCC, hepatocellular carcinoma; HCC-SN, supernatants from cultures of primary HCC cells; PD-L1, programmed death ligand-1.

as well as HLA-DR and PD-L1 expression, in HCC-SN-exposed monocytes (figure 6F,G). Consistent with this in vitro observation, confocal microscopy demonstrated that, in human HCC tumour tissues, PKM2 was selectively and highly expressed by $PD\text{-}L1^+$ macrophages and was only weakly expressed by the $PD\text{-}L1^-$ stromal and hepatoma cells (figure 6H).

It is noteworthy that, besides serving as a key rate-limiting glycolytic enzyme, PKM2 can translocate into the nucleus to maintain HIF-1α stabilisation and STAT3 phosphorylation.[25–27] Indeed, silencing PKM2 expression in HCC-SN-exposed monocytes largely suppressed the activities of both HIF-1α and STAT3 (figure 6I). In support, suppressing the stabilisation of HIF-1α by inhibitor α-ketoglutarate significantly antagonised pluripotent polarisation of tumour macrophages (figure 6J,K), and the effect was comparable with that of PKM2 inhibition. In contrast, abolishing the activation of the STAT3 signal had no effect (figure 6J,K). These data indicate that PKM2/HIF-1α axis participates in pluripotent polarisation of tumour macrophages.

To investigate the impact of $PKM2^+$ macrophages on clinical features of human HCC, we collected and analysed clinical data on 91 patients with HCC (online supplemental table 1) and divided these subjects into two groups according to the median value of dual immunohistochemical staining $PKM2^+CD68^+$ cell density (figure 6L). We found a striking inverse association between $PKM2^+CD68^+$ cell density in HCC tumours and disease-free survival (p=0.019; figure 6M). The density of $PKM2^+CD68^+$ cells was also associated with tumour size (p=0.045), tumour, node, metastases stage (p=0.009) and cirrhosis (p=0.021; online supplemental table 6). In multivariate analysis, the number of $PKM2^+CD68^+$ cells was an independent prognostic factor for disease-free survival (p=0.048; online supplemental table 7).

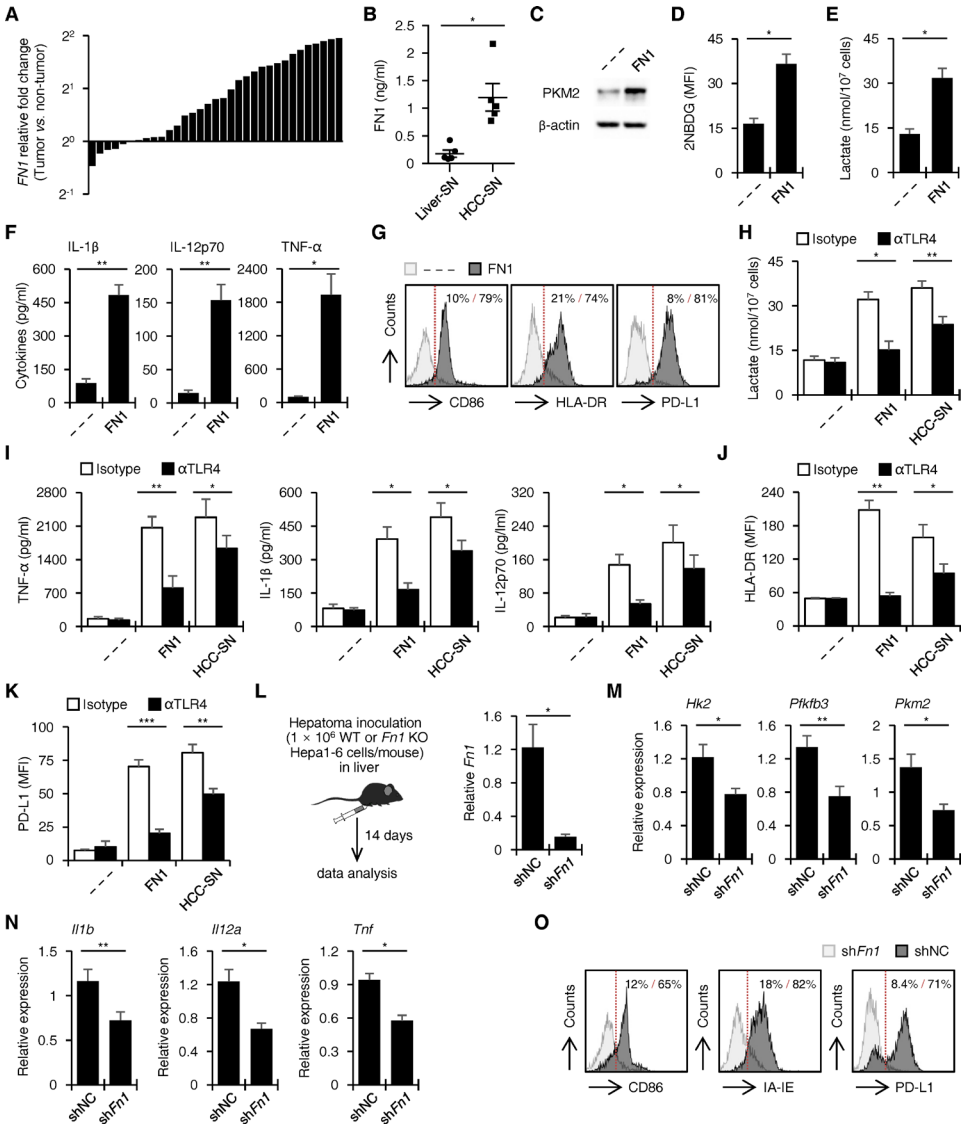

Figure 7 Tumour-derived FN1 facilitated sequential glycolysis, inflammatory cytokine production and PD-L1 expression in macrophages. (A) Relative expression of *FN1* in tumour tissue and paired non-tumoural liver tissue (n=33). (B) FN1 concentrations in liver-SN and HCC-SN (n=5). (C–G) Treatment of FN1 led to increases of PKM2 expression (C), 2-NBDG incorporation (D), lactate production (E), inflammatory cytokine production (F), as well as CD86, HLA-DR and PD-L1 expression (G), in blood $CD14^+$ cells. (H–K) Effect of TLR4 blockade on FN1-elicited or HCC-SN-elicited lactate production (H), cytokine production (I), HLA-DR expression (J) and PD-L1 expression (K) in blood $CD14^+$ cells (each n=4). (L–O) Knock-down of *Fn1* (L) in Hepa1-6 hepatoma suppressed glycolytic enzyme expression (M), inflammatory cytokine expression (N), as well as CD86, IA-IE and PD-L1 expressions (O), in tumour macrophages (each n=5). Results are expressed as the mean±SEM. *P<0.05, **p<0.01, ***p<0.001. 2-NBDG, 2-(N-[7-nitrobenz-2-oxa-1,3-diazol-4-yl] amino)-2-deoxyglucose; FN1, fibronectin 1; HCC-SN, supernatants from cultures of primary HCC cells; PD-L1, programmed death ligand-1.

FN1 derived from hepatoma cells orchestrates glycolytic metabolism-elicited macrophage polarisation

In some cancer patients, high levels of FN1 are associated with poor prognosis.[28–30] We detected extremely higher expression of *FN1* in HCC tumour tissues compared with paired non-tumoural liver tissues (figure 7A). Analogously, increased level of FN1 was detected in HCC-SN, as compared with liver-SN (figure 7B). These findings prompted us to investigate whether FN1 contributed to HCC-SN-induced metabolic reprogramming and pluripotent polarisation of macrophages. Stimulation for 24 hours with recombinant FN1 elicited upregulation of the key rate-limiting glycolytic enzyme PKM2 in monocytes (figure 7C) and increased activities of those cells to incorporate and utilise glucose (figure 7D,E). Similarly, recombinant FN1 mimicked the effect of HCC-SN to induce production of IL-1β, IL-12p70 and TNF-α and expression of HLA-DR and PD-L1 in monocytes (figure 7F,G).

It is noteworthy that TLR4 is an important physiological receptor of FN1.[31–33] We therefore used an antibody to specifically shield the TLR4 signals in the presence of either recombinant FN1 or HCC-SN. As expected, pretreatment of monocytes with this anti-TLR4 mAb effectively suppressed their glycolytic metabolism, cytokine production and HLA-DR and PD-L1 expression in these cells stimulated by exposure to HCC-SN or recombinant FN1 (figure 7H–K). Moreover, we knocked down the *FN1* gene in human hepatoma cells Huh7 and in mouse Hepa1-6 hepatoma (figure 7L and online supplemental figure 6A). These treatments significantly impaired the abilities

of glycolysis and cytokine production, as well as the expression of CD86, HLA-DR and PD-L1, in macrophages in vitro and in hepatoma-bearing mice (figure 7M–O and online supplemental figure 6B-D). Thus, FN1 derived from hepatoma cells may represent an important factor resulted in glycolytic metabolism-elicited macrophage polarisation.

DISCUSSION

Our present study provides evidence that PD-L1 expressed by host macrophages represents a mechanism involved in cancer immune privilege and reflects an existence of classical innate antitumourigenic immunity. PD-L1 blockade liberates antitumourigenic activity of macrophages.

It is noteworthy that PD-L1 leads to the exhaustion of tumour-specific T cells.[9 34] Thus, it is reasonable to assume that PD-L1 expression might correlate with clinical response to anti-PD-1/PD-L1 treatment. However, several clinical studies have shown that, although the underlying mechanism is still unclear, PD-L1 expressed by cancer cells and host stromal cells represents different biological and clinical significance.[8 9] In fact, PD-L1 expressed by cancer cells can be regulated by many biological processes, including chromosomal rearrangements, copy number alterations, oncogenic pathway dysregulation and epigenetic modulation.[35–37] Nevertheless, PD-L1 expressed by host cells is induced mainly by the local tumour environments.[8 10] In this study, we show that PD-L1$^+$ host macrophages, representing the major source of PD-L1 in HCC tumours, exhibit a glycolytic phenotype. We demonstrate that suppression of glycolytic metabolism ex vivo abrogates PD-L1 expression in tumour macrophages. Interestingly, suppression of PD-L1 by specific Ab abolishes PD-L1-dominant immune privilege and additionally enhances glycolytic macrophage-mediated specific T cell cytotoxicity. It is plausible that it is not PD-L1 per se, but rather the cells that express PD-L1, that determine the therapeutic efficiency of anti-PD-1/PD-L1 treatment.[38] This notion is supported by our observation that PD-L1$^+$ glycolytic macrophages exhibit an HLA-DR^{high}CD86^{high} phenotype and produce significant antitumourigenic IL-12p70.

Despite recent success in demonstrating the importance of glycolysis in sustaining the polarisation of classical activated macrophages (M1) and OXPHOS in regulating alternative activation of macrophages (M2),[13] the direct metabolic mechanisms tumour-infiltrating macrophages during cancer progression are still unclear. Our data show that, in HCC tumour tissues, glycolytic metabolism is involved in PD-L1$^+$ macrophage polarisation, whereas OXPHOS is restricted to the energy needs in PD-L1$^-$ macrophages. More importantly, we show that glycolytic metabolism simultaneously controls antitumourigenic and protumourigenic activities of PD-L1$^+$ macrophages. On the one hand, suppression of glycolytic metabolism reduces the PD-L1 expressed by tumour macrophages, which in turn restores the abilities of tumour T cells to produce IFN-γ and kill autologous hepatoma cells. On the other hand, inhibition of glycolytic metabolism also reduces the expression of MHC class II molecule HLA-DR and costimulatory CD86, as well as the production of antitumourigenic IL-12p70, by tumour macrophages. Therefore, although targeting glycolytic metabolism of macrophages abrogates PD-L1-mediated immune privilege, this strategy also suppresses antitumourigenic innate immunity. This hypothesis is compatible with previous studies showing that glycolytic metabolism also contributes to the effector function of cytotoxic T and NK cells.[39 40]

In addition to its role in glycolysis, PKM2 supports the function of transcription factors including HIF-1α and STATs.[25–27] Our study shows that PKM2/HIF-1α axis has a significant role in regulating PD-L1 expression in tumour macrophages. Consistent with this, the density of PKM2$^+$CD68$^+$ cells in tumour tissues was correlated with advanced disease stages and poor survival in patients with HCC. It should be emphasised that, although the increase of PKM2$^+$CD68$^+$ cells in tumour tissue predicts a poor prognosis, this situation can be used as a predictive biomarker of benefit from anti-PD-1/PD-L1 treatment, because blocking PD-L1 signal liberates the antitumourigenic activity of PKM2$^+$CD68$^+$ cells. Therefore, studying the mechanisms that can selectively modulate or reverse the phenotype of glycolytic macrophages might provide a precise strategy for anticancer therapy.

In patients with cancer, FN-1 expression is usually higher in malignant tumour than in corresponding benign or normal tissue.[28–30] Experimental studies have revealed that FN-1 does not only promote tumour growth and metastasis, but also modulates the functions of immune cells.[31–33] In support of those findings, the results of three sets of experiments in our investigation provide evidence that FN-1 is an important factor that is produced by hepatoma cells to trigger glycolytic metabolism-mediated pluripotent polarisation of macrophages. First, recombinant FN-1 is able to mimic the ability of HCC-SN to induce the pluripotent polarisation of macrophages. Second, pretreatment with an anti-TLR4 mAb to antagonise the interactions between FN-1 and its receptors partially suppressed proinflammatory responses and subsequent PD-L1 expression in HCC-SN-exposed monocytes. Third, silencing of FN-1 in Hepa1-6 hepatoma-bearing mice attenuated the glycolysis, cytokine production and PD-L1 expression in tumour macrophages in vivo. Therefore, FN-1 generated in hepatoma environments may constitute an important mediator of glycolytic metabolism-elicited pluripotent polarisation of macrophages. Notably, besides producing FN-1, hepatoma cells also secrete molecules (eg, hyaluronan fragments), which also contributed to the expression of PD-L1 in macrophages.[41] Studying the mechanisms that can selectively modulate the functional activities of macrophages might provide a novel strategy for anticancer therapy.

In the current study, FN-1 derived from cancer cells promotes glycolytic activation of macrophages by triggering TLR4, and thereby induce the macrophages to express significant amount of PD-L1, which in turn impaired the intrinsic antitumourigenic activities of glycolytic macrophages. Our results provide important insights into the significance about how glycolytic macrophages in tumours may perform a suppressive role by stimulating PD-L1 expression, which would be helpful for the rational design of novel immune-based anticancer therapies.

Author affiliations
[1]Interventional Radiology Center, Zhuhai Precision Medicine Center, Zhuhai People's Hospital, Zhuhai Hospital Affiliated with Jinan University, Zhuhai, Guangdong, China
[2]Department of Immunology, Key Laboratory of Human Functional Genomics of Jiangsu Province, Gusu School, Nanjing Medical University, Nanjing, Jiangsu, China
[3]Jiangsu Key Lab of Cancer Biomarkers, Prevention and Treatment, Collaborative Innovation Center for Cancer Personalized Medicine, Nanjing, Jiangsu, China
[4]Jiangsu Institute of Clinical Immunology, The First Affiliated Hospital of Soochow University, Suzhou, Jiangsu, China

Contributors All authors have full access to all data used in the study and take responsibility for the integrity of the data and the accuracy of the data analysis. L-GL, Z-LZ, X-YW, B-YL, J-YL, SL and G-BZ acquired experimental data. L-GL, Z-LZ and YC provided administrative, technical or material support. L-GL, G-BZ, M-XZ and YC were involved in study design and obtaining funding.

Funding This work was supported by project grants from the National Key Research and Development Program of China (2017YFA0205200), the National Natural Science Foundation of China (82071767, 81772602, 91742105, 91942309), the Jiangsu Provincial Key Research Development Program of China (BE2018750), the Key Laboratory of Emergency and Trauma, Ministry of Education (KLET-201913), the Research Start Project of Zhuhai People's Hospital (No.2020ycqd001), and the Science and Technology Development Fund, Macau SAR (0011/2019/AKP).

Competing interests None declared.

Patient consent for publication Not applicable.

Ethics approval All human samples were anonymously coded in accordance with local ethical guidelines (as stipulated by the Declaration of Helsinki). Written informed consent was obtained from each patient, and the study protocol was approved by the Review Board of the First Affiliated Hospital of Nanjing Medical University (GZR2020/09). Participants gave informed consent to participate in the study before taking part.

Provenance and peer review Not commissioned; externally peer reviewed.

Data availability statement All data relevant to the study are included in the article or uploaded as supplementary information.

ORCID iD

Yun Chen http://orcid.org/0000-0002-4118-362X

REFERENCES

1 Chen L, Han X. Anti-Pd-1/Pd-L1 therapy of human cancer: past, present, and future. *J Clin Invest* 2015;125:3384–91.
2 Zou W, Wolchok JD, Chen L. Pd-L1 (B7-H1) and PD-1 pathway blockade for cancer therapy: mechanisms, response biomarkers, and combinations. *Sci Transl Med* 2016;8:328rv324.
3 Jia L, Zhang Q, Zhang R. Pd-1/Pd-L1 pathway blockade works as an effective and practical therapy for cancer immunotherapy. *Cancer Biol Med* 2018;15:116–23.
4 Han Y, Liu D, Li L. Pd-1/Pd-L1 pathway: current researches in cancer. *Am J Cancer Res* 2020;10:727–42.
5 Keir ME, Butte MJ, Freeman GJ, *et al*. Pd-1 and its ligands in tolerance and immunity. *Annu Rev Immunol* 2008;26:677–704.
6 Doroshow DB, Bhalla S, Beasley MB, *et al*. Pd-L1 as a biomarker of response to immune-checkpoint inhibitors. *Nat Rev Clin Oncol* 2021;18:345–62.
7 Francisco LM, Salinas VH, Brown KE, *et al*. Pd-L1 regulates the development, maintenance, and function of induced regulatory T cells. *J Exp Med* 2009;206:3015–29.
8 Tang H, Liang Y, Anders RA, *et al*. Pd-L1 on host cells is essential for PD-L1 blockade-mediated tumor regression. *J Clin Invest* 2018;128:580–8.
9 Zhang X, Cheng C, Hou J, *et al*. Distinct contribution of PD-L1 suppression by spatial expression of PD-L1 on tumor and non-tumor cells. *Cell Mol Immunol* 2019;16:392–400.
10 Lin H, Wei S, Hurt EM, *et al*. Host expression of PD-L1 determines efficacy of PD-L1 pathway blockade-mediated tumor regression. *J Clin Invest* 2018;128:805–15.
11 Wei Y, Lao X-M, Xiao X, *et al*. Plasma cell polarization to the immunoglobulin G phenotype in hepatocellular carcinomas involves epigenetic alterations and promotes hepatoma progression in mice. *Gastroenterology* 2019;156:1890–904.
12 Kuang D-M, Wu Y, Chen N, *et al*. Tumor-Derived hyaluronan induces formation of immunosuppressive macrophages through transient early activation of monocytes. *Blood* 2007;110:587–95.
13 Yang M, McKay D, Pollard JW, *et al*. Diverse functions of macrophages in different tumor microenvironments. *Cancer Res* 2018;78:5492–503.
14 Van den Bossche J, O'Neill LA, Menon D. Macrophage Immunometabolism: where are we (going)? *Trends Immunol* 2017;38:395–406.
15 Vitale I, Manic G, Coussens LM, *et al*. Macrophages and metabolism in the tumor microenvironment. *Cell Metab* 2019;30:36–50.
16 O'Neill LAJ, Pearce EJ. Immunometabolism governs dendritic cell and macrophage function. *J Exp Med* 2016;213:15–23.
17 Llovet JM, Kelley RK, Villanueva A, *et al*. Hepatocellular carcinoma. *Nat Rev Dis Primers* 2021;7:6.
18 Chen M-M, Xiao X, Lao X-M, *et al*. Polarization of tissue-resident TFH-like cells in human hepatoma bridges innate monocyte inflammation and M2b macrophage polarization. *Cancer Discov* 2016;6:1182–95.
19 Schmidt CA, Fisher-Wellman KH, Neufer PD. From ocr and ECAR to energy: perspectives on the design and interpretation of bioenergetics studies. *J Biol Chem* 2021;297:101140.
20 Van den Bossche J, van der Windt GJW. Fatty acid oxidation in macrophages and T cells: time for reassessment? *Cell Metab* 2018;28:538–40.
21 Symersky J, Osowski D, Walters DE, *et al*. Oligomycin frames a common drug-binding site in the ATP synthase. *Proc Natl Acad Sci U S A* 2012;109:13961–5.
22 Watkins SK, Egilmez NK, Suttles J, *et al*. Il-12 rapidly alters the functional profile of tumor-associated and tumor-infiltrating macrophages in vitro and in vivo. *J Immunol* 2007;178:1357–62.
23 Vignali DAA, Kuchroo VK. Il-12 family cytokines: immunological playmakers. *Nat Immunol* 2012;13:722–8.
24 Zong Z, Zou J, Mao R, *et al*. M1 macrophages induce PD-L1 expression in hepatocellular carcinoma cells through IL-1β signaling. *Front Immunol* 2019;10:1643.
25 Palsson-McDermott EM, Curtis AM, Goel G, *et al*. Pyruvate kinase M2 regulates HIF-1α activity and IL-1β induction and is a critical determinant of the Warburg effect in LPS-activated macrophages. *Cell Metab* 2015;21:65–80.
26 Shirai T, Nazarewicz RR, Wallis BB, *et al*. The glycolytic enzyme PKM2 bridges metabolic and inflammatory dysfunction in coronary artery disease. *J Exp Med* 2016;213:337–54.
27 Damasceno LEA, Prado DS, Veras FP, *et al*. Pkm2 promotes Th17 cell differentiation and autoimmune inflammation by fine-tuning STAT3 activation. *J Exp Med* 2020;217:e20190613.
28 Bae YK, Kim A, Kim MK, *et al*. Fibronectin expression in carcinoma cells correlates with tumor aggressiveness and poor clinical outcome in patients with invasive breast cancer. *Hum Pathol* 2013;44:2028–37.
29 Waalkes S, Atschekzei F, Kramer MW, *et al*. Fibronectin 1 mRNA expression correlates with advanced disease in renal cancer. *BMC Cancer* 2010;10:503.
30 Li B, Shen W, Peng H, *et al*. Fibronectin 1 promotes melanoma proliferation and metastasis by inhibiting apoptosis and regulating EMT. *Onco Targets Ther* 2019;12:3207–21.
31 Julier Z, Martino MM, de Titta A, *et al*. The TLR4 agonist fibronectin extra domain A is cryptic, exposed by elastase-2; use in a fibrin matrix cancer vaccine. *Sci Rep* 2015;5:8569.
32 Okamura Y, Watari M, Jerud ES, *et al*. The extra domain A of fibronectin activates Toll-like receptor 4. *J Biol Chem* 2001;276:10229–33.
33 Prakash P, Kulkarni PP, Lentz SR, *et al*. Cellular fibronectin containing extra domain a promotes arterial thrombosis in mice through platelet Toll-like receptor 4. *Blood* 2015;125:3164–72.
34 Wei Y, Zhao Q, Gao Z, *et al*. The local immune landscape determines tumor PD-L1 heterogeneity and sensitivity to therapy. *J Clin Invest* 2019;129:3347–60.
35 Yu G, Wu Y, Wang W, *et al*. Low-Dose decitabine enhances the effect of PD-1 blockade in colorectal cancer with microsatellite stability by re-modulating the tumor microenvironment. *Cell Mol Immunol* 2019;16:401–9.
36 George J, Saito M, Tsuta K, *et al*. Genomic Amplification of *CD274* (PD-L1) in Small-Cell Lung Cancer. *Clin Cancer Res* 2017;23:1220–6.
37 Li X, Song W, Shao C, *et al*. Emerging predictors of the response to the blockade of immune checkpoints in cancer therapy. *Cell Mol Immunol* 2019;16:28–39.
38 Wei Y, Xiao X, Lao X-M, *et al*. Immune landscape and therapeutic strategies: new insights into PD-L1 in tumors. *Cell Mol Life Sci* 2021;78:867–87.
39 Finlay D, Cantrell DA. Metabolism, migration and memory in cytotoxic T cells. *Nat Rev Immunol* 2011;11:109–17.
40 Mah AY, Rashidi A, Keppel MP, *et al*. Glycolytic requirement for NK cell cytotoxicity and cytomegalovirus control. *JCI Insight* 2017;2:e95128.
41 Chen D-P, Ning W-R, Jiang Z-Z, *et al*. Glycolytic activation of peritumoral monocytes fosters immune privilege via the PFKFB3-PD-L1 axis in human hepatocellular carcinoma. *J Hepatol* 2019;71:333–43.

Supplementary Materials and methods

Isolation of mononuclear cells from peripheral blood and tissues

Peripheral leukocytes were isolated by Ficoll density gradient centrifugation. Thereafter, the mononuclear cells were washed and resuspended in RPMI 1640 supplemented with 10% FBS. Monocytes/macrophages and T cells were purified from the leukocytes using a MACS column purification system (Miltenyi Biotec). Human $CD8^+$ T cells, PD-$L1^+$ and PD-$L1^-$ monocytes/macrophages, HLA-DR^{high} and HLA-DR^{low} monocytes/macrophages, as well as mouse $F4/80^+$ macrophages and $CD8^+$ T cells were further sorted by FACS (MoFlo, Beckman Coulter). These cells were used in subsequent experiments.

Animal experiments

All mice were maintained under specific pathogen-free conditions in the animal facilities of the First Affiliated Hospital of Nanjing Medical. All mice were randomly grouped. Animal experiments were performed with the approval of the Institutional Animal Care and Use Committee of the First Affiliated Hospital of Nanjing Medical. 1×10^6 mouse hepatoma Hepa1-6 cells in 25 μl of Matrigel (Corning) were injected under the hepatic capsule of 5–7-week-old female C57/BL6 mice. In some experiments, Hepa1-6 cells were pre-transfected with shNC or sh*Fn1* by lentiviral vectors delivery system. The detailed procedures of the animal experiments are shown in figure 1J, figure 4C, and figure 7L.

Immunohistochemistry and immunofluorescence

Paraffin-embedded and formalin-fixed samples were cut into 5-μm sections, followed by procedures for immunohistochemistry. After incubation with primary antibody against human CD68, PD-L1, HLA-DR, and PKM2, sections were stained with corresponding secondary antibodies and visualized in an Envision System. For immunofluorescence analysis of patient samples, frozen sections were initially incubated with mouse anti-human CD68 and rabbit anti-human PD-L1; or mouse anti-human CD68, rabbit anti-human PKM2 and rabbit anti-human PD-L1. Thereafter, sections were stained with Alexa Fluor 488-conjugated donkey anti-rabbit IgG and Alexa Fluor 555-conjugated donkey anti-mouse IgG (Invitrogen); or Alexa Fluor 488-conjugated donkey anti-mouse IgG, Alexa Fluor 555-conjugated donkey anti-rabbit IgG, and Cyanine 5-conjugated streptavidin detect biotinylated corresponding secondary antibodies anti-

rabbit IgG. Nuclei were counterstained with DAPI. Immunofluorescence staining images were visualized by confocal microscopy (LSM 880, AxioObserver; Carl Zeiss, Oberkochen, Germany).

Evaluation of immunohistochemical variables

Analysis was performed by two independent observers who were blinded to the clinical outcomes. At low-power field (× 100), the tissue sections were screened, and the 5 most representative fields were selected using a Leica DM IRB inverted research microscope (Leica, Wetzlar, Germany). For evaluating the density of tissue-infiltrating $CD68^{+}PKM2^{+}$ cells, the respective areas of HCC tissues were then scanned at × 400 magnification (0.146 mm^2 per field). The number of nucleated $PKM2^{high}$ cells in each area was then counted manually and expressed as cells per field. The $PKM2^{high}$ cells that were negative for CD68 were excluded from counting. Positively stained cells that are smaller than the size of circulating monocytes/macrophages (15 μm) were excluded from counting. There was a significant linear correlation between the counting data of two independent observers ($P= 2.77 \times 10^{-24}$), and the average of counts by 2 investigators was applied in the following analysis to minimize interobserver variability.

Flow cytometry (FACS)

Monocytes/macrophages and T cells from peripheral blood, tissues, or ex vivo culture were stained with fluorochrome-conjugated antibodies and then analyzed by FACS. In some cases, T cells from ex vivo culture system were stimulated with Leukocyte Activation Cocktail (BD Bioscience) at 37°C for 5 hours. Thereafter, the cells were stained with surface markers, fixed and permeabilized with IntraPrep reagent (Beckman Coulter), and finally stained with intracellular markers. Data were acquired using a Gallios flow cytometer (Beckman Coulter).

Real-time polymerase chain reaction (PCR)

Trizol reagent (Invitrogen) was used to isolate total RNA of cells or tissue. Aliquots (2 μg) of the RNA were reverse-transcribed using MMLV reverse transcriptase. The PCR was performed in triplicate using Hieff qPCR SYBR Green Master Mix in a Roche LightCycler 480 System.

Immunoblotting

Monocytes/macrophages from in vitro culture system were washed three times with PBS and

the pellets were resuspended in lysis buffer for 20 minutes on ice. After centrifugation at 10,000 g for 10 minutes, the supernatants were dissolved in Laemmli sample buffer and heated at 95 °C for 5 minutes. Equal amount of cellular proteins was separated on 10% SDS–polyacrylamide gel electrophoresis and electrotransfered to nitrocellulose membranes. The membranes were blocked with 3% bovine serum albumin, and the presence of indicated protein on the blots was detected with specific antibodies and commercial ECL kit.

Glucose uptake assay

Purified monocytes/macrophages were starved of glucose by incubation for 1 hour in PBS and then stained with 2-NBDG for 30 minutes at 37 °C and subjected to FACS analysis.

Extracellular acidification (ECAR) analyses

Measurement of the ECAR of monocytes/macrophages was done using an XF-24 Extracellular Flux Analyzer (Seahorse Bioscience). HLA-DR^{high} and HLA-DR^{low} monocytes/macrophages isolated from tissue or macrophages cultured in vitro were suspended in XF Base Medium Minimal DMEM (pH 7.4) with L-Glutamine (2 mM) and then placed on a cell culture microplate (2×10^5 cells/well; XF-24, Seahorse Bioscience). Glucose (10 mM), oligomycin A (1 μM), and 2-DG (50 mM) were added to the cells during performing real-time measurement of the ECAR.

Lactate assay

The supernatants of monocytes/macrophages were collected from ex vivo or in vitro culture systems. Concentrations of the lactate in the supernatants were detected using L-lactate assay kit according to the manufacturers' instructions (Eton bioscience).

In vitro and ex vivo culture of monocytes/macrophages

Monocytes/macrophages, PD-L1$^+$ or HLA-DR^{high} monocytes/macrophages isolated from HCC tissues were left untreated or treated with 2-DG (25 mM), oligomycin (Oym, 0.5 μM), etomoxir (ETO, 50 μM), or with neutralizing antibodies against human TNF-α (10 μg/mL), IL-1β (10 μg/mL), IL-6 (40 μg/mL), IL-12 (10 μg/mL). In some experiments, purified monocytes from human blood were untreated or treated with human recombinant TNF-α (20 ng/ml), IL-1β (10 ng/ml), IL-6 (40 ng/ml), IL-12 (10 ng/ml), or with 30% primary liver-SN or primary HCC-SN,

or FN1 (20 μg/ml) in the presence or absence of 2-DG, 3-PO (30 nM), 3-BP (20 nM), ML-265 (50 μM), α-KG (20 μg/mL), WP1066 (1 ug/ml), or antibody against TLR-4 (20 μg/ml). In other experiments, monocytes were pre-transfected with 300 nM negative control siRNA, or PKM2-specific siRNA (sense: 5'-CCU GUA UGU CAA UAA ACA ACA-3'; antisense: 5'-UUG UUU AUU GAC AUA CAG GUA-3') using P3 primary cell 4D-Nucleofector X kit (V4XP-3024, Lonza) before exposure to HCC-SN. All siRNA duplexes were purchased from GenePharma.

Ex vivo T cell culture system

$CD8^+$ T cells, PD-$L1^-$ and PD-$L1^+$ monocytes/macrophages were isolated from human HCC tumors by FACS-sorting. PD-$L1^+$ monocytes/macrophages were pretreated with glycolysis inhibitor 2-DG for 24 hours. Thereafter, 1×10^5 T cells were left untreated or were cultured with autologous PD-$L1^-$ or PD-$L1^+$ monocytes/macrophages (5:1) in the presence or absence of a specific blocking antibody against PD-L1 (20 μg/mL) for 20 hours. Meanwhile, 25 μg/ml of tumor mass lysates were added to trigger tumor specific T cell response. In some cases, T cells and PD-$L1^+$ monocytes/macrophages were cocultured with specific blocking antibodies against IL-12 (10 μg/mL) or HLA-DR (20 μg/mL) in the presence of PD-L1 blocking antibody.

Enzyme-linked immunospot assay (ELISpot)

ELISpot assays were performed using commercial kits (BD Bioscience) according to the manufacturer's instructions. In brief, 96-well nitrocellulose plates (Millipore) were coated with 5 μg/ml anti–human IFN-γ capture antibody at 4°C overnight. The wells were then washed and blocked for 2 hours at room temperature with 10% FBS-RPMI 1640 medium. 1×10^5 purified $CD8^+$ T cells from human HCC tissues were left untreated or were cultured with autologous monocytes/macrophages for 20 hours in the plate. After wash, the plates were incubated with 2 μg/ml of biotinylated anti–human IFN-γ detection antibody and developed with streptavidin–horseradish peroxidase, followed by the addition of 3-amino-9-ethylcarbazole substrate reagent. In some experiments, Mock or PD-L1 HEK293T transfectants were primary pretreated with 10 μg/mL mitomycin C for 20 minutes to abolish the growth or cytokine production activity of cells. Thereafter, purified $CD8^+$ T cells were left untreated or cultured for 24 hours with indicated mitomycin C–treated cells in the presence or absence of 10 ng/mL human recombinant IL-12 antibody (eBioscience). The production of IFN-γ by tumor $CD8^+$ T cells

was determined by ELISpot Assay. The images were scanned with an ELISpot reader (CTL), and spot numbers were counted manually.

Ex vivo tumor-specific T cell cytotoxicity assay

$CD8^+$ T cells and macrophages were isolated from mice Hepa1-6 tumors. Macrophages were pretreated with glycolysis inhibitor 2-DG for 24 hours. 1×10^5 $CD8^+$ T cells were left untreated or were cultured with autologous macrophages and CFSE-labelled Hepa1-6 cells (10:2:1) in the presence or absence of a specific blocking antibody against PD-L1 (20 μg/mL) for 12 hours. Meanwhile, 25 μg/ml of tumor mass lysates were added to trigger tumor specific T cell response. Propidum $iodide^+$ apoptotic tumor cells were analyzed by flow cytometry.

Enzyme-linked immunosorbent assay (ELISA)

Concentrations of the cytokines TNF-α, IL-1β, IL-6, and IL-12p70 in the supernatants from in vitro or ex vivo culture systems were detected using ELISA kits according to the manufacturers' instructions (eBioscience).

Preparation of culture supernatant from primary tumors

Culture supernatants were acquired by culture of completely digested HCC tumor. All specimens were from individuals without concurrent autoimmune disease, HBV, HCV, HIV, or syphilis. The digested tumor or liver cells were washed in medium containing polymyxin B (20 μg/mL; Sigma-Aldrich) to exclude endotoxin contamination. Thereafter, 1×10^7 digested cells were resuspended in 10 mL of complete medium and cultured in 100-mm dishes. In some experiments, Huh7 cells were pre-transfected with shNC or shFN1 by lentiviral vectors delivery system. Tumor culture supernatants were prepared by plating 5×10^6 tumor cells in 10 mL complete medium in 100-mm dishes. After 2 days, the supernatants were harvested, centrifuged, and stored at −80°C.

Construction of PD-L1 stable cell lines

The PD-L1 gene was amplified by PCR from human cDNA and confirmed by DNA sequencing. The gene fragment was inserted into retrovirus vector pBABE-puro and cotransfected into the package cell HEK293T with helper virus vector pBABE-ampho in the context of Lipofectamine (Invitrogen). The supernatant of these HEK293T cells was used to infect original HEK293T

cells. The cell lines stably expressing PD-L1 and the mock transfectant were selected with puromycin (1 μg/mL, Sigma-Aldrich).

Supplementary Tables

Table S1. Clinical characteristics of HCC patients

Patients characteristics	**Cohort 1**	**Cohort 2**
No. of patients	91	93
Age, years (median, range)	51, 19–81	50.7, 27–78
Gender (male: female)	76:15	71:22
HBsAg (negative: positive)	14:77	23:70
Cirrhosis (absent: present)	24:67	28:65
ALT, U/L (median, range)	41.4, 12.3–533.7	39.4, 9.9–453.7
AFP, ng/ml (≤ 25: > 25)	43:48	47:46
Tumor size, cm (≤ 5: > 5)	37:54	38:55
Tumor multiplicity (solitary: multiple)	71:20	71:22
Vascular invasion (absent: present)	63:28	64:29
TNM stage (I+II: III+IV)	43:48	63:30
Tumor differentiation (I+II: III+IV)	62:29	58:35
Fibrous capsule (absent: present)	35:56	39:54
Tumor $PKM2^{+}CD68^{+}$ cells density (median, range)	90, 26–211	N/A

Abbreviations: HBsAg, hepatitis B surface antigen; AFP, alpha fetoprotein; ALT, alanine aminotransferase; TNM, tumor-node-metastasis; N/A, not applicable.

Note: Patients in cohort 1 contributed to the paraffin embedded samples for immunohistochemical staining that were used in analyses of cell distribution, correlation, and patient prognosis; patients in cohort 2 contributed fresh samples.

Table S2. Fluorochrome-conjugated antibodies used in flow cytometry

Antibody	Supplier	Catalogue	RRID
Anti-Human CD14 Antibody, AF 700, Clone M5E2	BD Biosciences	557923	AB_396944
Anti-Human CD23 Antibody, APC Conjugated, Clone M-L233	BD Biosciences	558690	AB_1645456
Anti-Human CD3 Antibody, AF 700, Clone OKT3	eBioscience	56-0037-42	AB_10714978
Anti-Human CD15 Antibody, eFluor 450, Clone MMA	eBioscience	48-0158-42	AB_1907348
Anti-Human CD19 Antibody, PE-CY7, Clone J4.119	Beckman Coulter	PM IM 3628U	NA
Anti-Human CD56 Antibody, PE-CY7, Clone N901	Beckman Coulter	A21692	AB_2892144
Anti-Human CD45 Antibody, KO, Clone J.33	Beckman Coulter	PN A96416	NA
Anti-Human CD86 Antibody, PE, Clone HA5.2B7	Beckman Coulter	IM2729U	NA
Anti-Human CD163 Antibody, PE, Clone GHI/61	eBioscience	12-1639-42	AB_1963570
Anti-Human CD206 Antibody, PE/Cy7, Clone 15-2	Biolegend	321124	AB_10933248
Anti-Human CD274 (PD-L1) Antibody, PE, Clone MIH1	eBioscience	12-5983-42	AB_11042286
Anti-Human CD274 (PD-L1) Antibody, PE-Cy7, Clone MIH1	BD Biosciences	558017	AB_396986
Anti-Human Glut1 Antibody, APC, Clone 202915	BD Biosciences	FAB1418A	AB_1207948
Anti-Human HLA-DR Antibody, PE-CF594, Clone G46-6	BD Biosciences	562304	AB_11154415
Anti-Mouse CD3 Antibody, AF 700, Clone 17A2	eBioscience	56-0032-82	AB_529507
Anti-Mouse CD8a Antibody, FITC, Clone 53-6.7	Invitrogen	11-0081-82	AB_464915
Anti-Mouse CD45 Antibody, BV 570, Clone 30-F11	Biolegend	103136	AB_2562612

Antibody	**Supplier**	**Catalogue**	**RRID**
Anti-Mouse CD86 Antibody, FITC, Clone GL-1	Biolegend	105005	AB_313148
Anti-Mouse CD274 Antibody, PE/Cyanine7, Clone 10F-9G2	Biolegend	124314	AB_10643573
Anti-Mouse F4/80 Antibody, APC, Clone BM8	Biolegend	123116	AB_893481
Anti-Mouse I-A/I-E Antibody, PE/Cyanine7, Clone M5/114.115.2	Biolegend	107629	AB_2290801
Anti-Mouse IFN-γ Antibody, ef450, Clone XMG1.2	eBioscience	48-7311-82	AB_1834366

Table S3. Antibodies for immunoblotting, IHC, and IF

Antibody	Supplier	Identifier
Antibodies for IHC/IF		
Anti-Human CD68 Antibody (PG-M1)	ZSBio	Cat# ZM-0464
Anti-Human CD8 Antibody	ZSBio	Cat# ZA-0508
Anti-Human HLA-DR Antibody (L243)	Biolegend	Cat# 307602; RRID:AB_314680
Anti-Human PD-L1 Antibody (E1L3N)	Cell Signaling Technology	Cat# 13684; RRID:AB_2687655
Anti-Human PKM2 Antibody (D78A4)	Cell Signaling Technology	Cat# 4053; RRID:AB_1904096
Cy 5-streptavidin	Invitrogen	Cat# 43-4316
Antibodies for immunoblotting		
Mouse Anti-Human HIF-1α	BD Biosciences	Cat# 610958; RRID:AB_398271
Rabbit Anti-Human HK2 (C64G5)	Cell Signaling Technology	Cat# 2867; RRID:AB_2232946
Rabbit Anti-Human LDHA Antibody	Proteintech	Cat# 19987-1-AP; RRID:AB_10646429
Rabbit Anti-Human PFKFB3	Proteintech	Cat# 13763-1-AP; RRID:AB_2162854
Rabbit Anti-Human PKM2	Cell Signaling Technology	Cat# 4053; RRID:AB_1904096
Rabbit Anti-Human Stat3 (Tyr705) (D3A7)	Cell Signaling Technology	Cat# 9145; RRID:AB_2491009
Mouse Anti-Stat3 Antibody (124H6)	Cell Signaling Technology	Cat# 9139; RRID:AB_331757
β-Actin (ACTB) Antibody (8H10)	Origene	Cat# TA310155; RRID:AB_10691552

Table S4. Primers for real-time PCR

Gene	Forward	Reverse
Primers for human gene		
IL6	TCAGCCCTGAGAAAGGAGACA	GATTTTCACCAGGCAAGTCTCC
TNF	AAGCCTGTAGCCCATGTTG	TGGTAGGAGACGGCGATG
IL1B	CGAATCTCCGACCACCACTAC	GATGAAGGGAAAGAAGGTGCTC
IL12A	GCTTCTTCATCAGGGACATCATC	GTCAGGGAGAAGTAGGAATGTGG
HK1	CGAGAGTGACCGATTAGCACT	AGACAGGAGGAAGGACACGTT
HK2	GATTGTCCGTAACATTCTCATCG	CAGGCAGTCACTCTCAATCTGAG
PFKFB3	CTCGCATCAACAGCTTTGAGG	TCAGTGTTTCCTGGAGGAGTC
ALDOA	AGATGAGTCCACTGGGAGCAT	AGATGAGTCCACTGGGAGCAT
GAPDH	GGAGTCAACGGATTTGGTCGT	TCTCGCTCCTGGAAGATGGT
PGK1	GGGTCGTTATGAGAGTCGACT	AGGTGGCTCATAAGGACTACC
ENO2	AACAGTGAAGCCTTGGAGCTG	TCCTCAATGGAGACCACAGGA
PKM	TCTGTACCATTGGCCCAGCTT	TGGCTGTGCGCACATTCTTGA
LDHA	GATTCCAGTGTGCCTGTATGG	CTACAGAGAGTCCAATAGCCC
CS	GGGCTGCAAGAACAAGACA	CTCCCTTTCTTACCTCCCCA
ACO2	AATGGATGTACTCGTTGGGC	ACAGCCTACTGGTGACTCGG
IDH2	AACCGTGACCAGACTGATGAC	ATGGTGGCACACTTGACAGC
OGDH	TTGGCTGGAAAACCCCAAAAG	TGTGCTTCTACCAGGGACTGT
SUCLA2	TTGCTTCAGGAGACTCAGCA	GTGAGCGAAAATATCCCAGG
SHDA	CGAACGTCTTCAGGTGCTTT	AAGAACATCGGAACTGCGAC
SHDB	CACAGATGCCTTCTCTGCAT	AAGGCTGGAGACAAACCTCA
FH	CCTCATCTGCTGCCTTCATT	GGAGGTGTGACAGAACGCAT
MDH2	TCGGCCCAGAACAATGCTAAA	GCGGCTTTGGTCTCGATGT
ACTB	GGATGCAGAAGGAGATCACT	CGATCCACACGGAGTACTTG
FN1	ACCTCGGTGTTGTAAGGTGG	CCATAAAGGGCAACCAAGAG
Primers for Mouse gene		
Il1b	GAAATGCCACCTTTTGACAGTG	TGGATGCTCTCATCAGGACAG
Il6	TGGAGTCACAGAAGGAGTGGCT	GCATAACGCACTAGGTTTGCCG
Il12a	TTCCTGCACTGCTGAAGACATC	CAAGGCACAGGGTCATCATCAA
Tnf	CCTGTAGCCCACGTCGTAG	GGGAGTAGACAAGGTACAACCC
Hk2	ATGATCGCCTGCTTATTCACG	CGCCTAGAAATCTCCAGAAGGG
Pfkfb3	ACGAAGATGCCGTTGGAACT	TCGACGGGCACCCAGAT
Pkm	TTGACTCTGCCCCCATCAC	GCAGGCCCAATGGTACAAAT
Actb	ACACCCGCCACCAGTTCGC	ATGGGGTACTTCAGGGTCAGGATA
Primers for si and sh		
si*PKM2*	CCUGUAUGUCAAUAAACAACA	UUGUUUAUUGACAUACAGGUA
shFN1	GGTTGTTATGACAATGGAA	TTCCATTGTCATAACAACC
sh*Fn1*	CTGGACCTGTCCAAGTAATTA	TAATTACTTGGACAGGTCCAG

Table S5. Recombinant proteins, peptides, chemicals, and critical commercial assays

Name	Supplier	Identifier
Recombinant proteins, peptides		
Human IL-1 beta/IL-1F2 antibody	R&D Systems	Cat# MAB601; RRID:AB_358545
Human IL-6 antibody, Clone 6708	R&D Systems	Cat# MAB206; RRID:AB_2127617
Human IL-12p70 antibody (24910)	R&D Systems	Cat# MAB219; RRID:AB_2123616
Human TNF-alpha antibody, Clone 28401	R&D Systems	Cat# MAB610; RRID:AB_2203945
Human TLR4 Affinity Purified antibody	R&D Systems	Cat# AF1478; RRID:AB_354816
Human CD274 (PD-L1) Antibody (MIH1)	eBioscience	Cat# 14-5983-82; RRID:AB_467784
InVivoMAb anti-mouse PD-L1 (B7-H1)	Bio X Cell	Cat# BE0101; RRID:AB_10949073
nVivoMab anti-mouse/rat IL-1β antibody	Bio X Cell	Cat# BE0246; RRID:AB_2687727
InVivoMab anti-mouse/rat/rabbit TNF-α antibody	Bio X Cell	Cat# BE0244; RRID:AB_2687725
Recombinant Human IL-1 beta/IL-1F2 Protein	R&D Systems	Cat# 201-LB-010
Recombinant Human IL-6 Protein	R&D Systems	Cat# 206-IL-010
Recombinant Human IL-12 Protein	R&D Systems	Cat# 219-IL-025
Recombinant Human TNF-alpha Protein	R&D Systems	Cat# 210-TA-020
Human Fibronectin Protein	R&D Systems	Cat# 1918-FN
Chemicals		
2-DG	Sigma-Aldrich	Cat# D8375 CAS: 154-17-6
2-NBDG	Sigma-Aldrich	Cat# 72987 CAS: 186689-07-6
3-BP	Sigma-Aldrich	Cat# 376817 CAS: 1113-59-3
3-PO	Merck Millipore	Cat# 525330 CAS: 18550-98-6
Etomoxir	Sigma-Aldrich	Cat# 236020 CAS: 828934-41-4
α-KG	Sigma-Aldrich	Cat# K2010 CAS: 22202-68-2

Chemicals		
ML-265	Cayman Chemical	Cat# 13942 CAS: 1221186-53-3
Oligomycin	Sigma-Aldrich	Cat# 495455 CAS: 1404-19-9
Propidium iodide	Sigma-Aldrich	Cat# P4170 CAS: 25535-16-4
WP1066	Sigma-Aldrich	Cat# 573097 CAS: 857064-38-1
Critical commercial assays		
IL-1β Human Uncoated ELISA kit	eBioscience	Cat# 88-7349
IL-6 Human Uncoated ELISA Kit	eBioscience	Cat# 88-7066
IL-12 p70 Human Uncoated ELISA kit	eBioscience	Cat# 88-7126
TNF-α Human Uncoated ELISA Kit	eBioscience	Cat# 88-7347
Human Fibronectin Platinum ELISA 10 x 96 tests Kit	Invitrogen	Cat# BMS2028TEN
Human IFN-γ ELISPOT Pair	BD Biosciences	Cat# 551873
IntraPrep reagent	Beckman Coulter	Cat# A07803
Hieff qPCR SYBR Green Master Mix	Yeasen	Cat# 11201ES03
Leukocyte Activation Cocktail	BD Biosciences	Cat# 550583
L-Lactate Assay Kit I -200 Assays	Eton bioscience	Cat# 1200012002
Trizol Reagent	Life Techonology	Cat# AM9738
XF Glycolysis Stress Test kit	Seahorse Bioscience	Cat# 102194-100
5X All-In-One RT MasterMix	abm	Cat# G492

Table S6. Association of tumor $PKM2^+$ $CD68^+$ cells with clinicopathological characteristics

Variables		Tumor $PKM2^+$ $CD68^+$ cells		
		High	Low	*p* value
Age, years	⩽ 51	28	28	0.895
	> 51	17	18	
Gender	Male	38	38	0.814
	Female	7	8	
HBsAg	Negative	8	6	0.531
	Positive	37	40	
Cirrhosis	Absent	7	17	**0.021**
	Present	38	29	
ALT, U/L	⩽ 40	23	21	0.602
	> 40	22	25	
AFP, ng/ml	⩽ 25	24	19	0.250
	> 25	21	27	
Tumor size, cm	⩽ 5	14	23	**0.045**
	> 5	32	22	
Tumor multiplicity	Solitary	35	36	0.956
	Multiple	10	10	
Vascular invasion	Absent	35	28	0.081
	Present	10	18	
TNM stage	I+II	15	28	**0.009**
	III+IV	30	18	
Tumor differentiation	I+II	31	31	0.878
	III+IV	14	15	
Fibrous capsule	Absent	15	20	0.320
	Present	30	26	

Abbreviations: HbsAg, hepatitis B surface antigen; ALT, alanine aminotransferase; AFP, α-fetoprotein; TNM, tumor-node-metastasis.

Table S7. Univariate and multivariate analysis of factors associated with disease-free survival of HCC patients

Variables				DFS			
				Univariate	Multivariate		
				p value	HR	95%CI of HR	*p* value
Age, years	> 51	vs.	⩽ 51	0.118			
Gender	female	vs.	male	0.246			
HBsAg	positive	vs.	negative	0.171			
Cirrhosis	present	vs.	absent	0.227			
ALT, U/L	> 40	vs.	⩽ 40	0.242			
AFP, ng/ml	> 25	vs.	⩽ 25	0.051			
Tumor size, cm	> 5	vs.	⩽ 5	0.071			
Tumor multiplicity	multiple	vs.	solitary	0.076			
Vascular invasion	present	vs.	absent	**0.004**	2.014	1.073–3.781	**0.029**
TNM stage	III+IV	vs.	I+II	**0.001**	5.395	2.583–11.270	**0.001**
Tumor differentiation	III+IV	vs.	I+II	**0.004**	0.349	0.194–0.628	**0.032**
Fibrous capsule	present	vs.	absent	0.535			
Tumor $PKM2^{+}CD68^{+}$ cells	high	vs.	low	**0.019**	1.823	1.005–3.308	**0.048**

Abbreviations: HBsAg, hepatitis B surface antigen; ALT, alanine aminotransferase; AFP, α-fetoprotein; TNM, tumor-node-metastasis; N/A, not applicable.

Figure S1

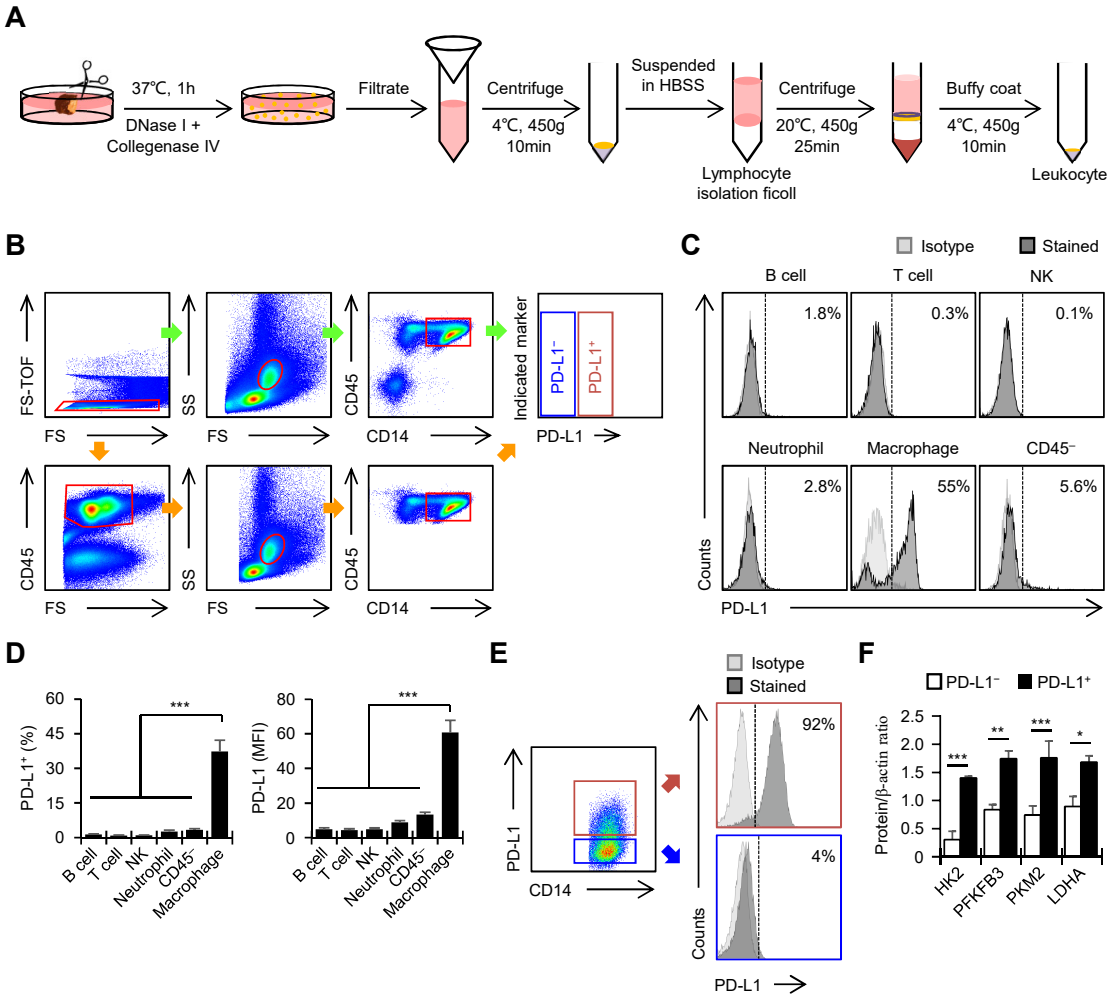

Figure S1. The expression of PD-L1 in human HCC tumors are mainly in macrophages. (A) Procedures for preparing single-cell leukocyte suspensions from human HCC tissues. **(B)** Representative plots of cells isolated from blood and tumor tissues showing that mononuclear cells from samples were first gated for singlets (FS-TOF vs. FS) and myeloid cells (SS vs. FS; green arrows), or alternatively, they were first gated for singlets (FS-TOF vs. FS) and leukocytes (CD45 vs. FS) then myeloid cells (SS vs. FS; orange arrows). Thereafter, the $CD45^+CD14^+$ macrophages were further divided into $PD\text{-}L1^-$ and $PD\text{-}1^+$ subsets. **(C and D)** FACS analysis of PD-L1 expression on B cells ($CD19^+$), T cells ($CD3^+CD56^-$), NK cells ($CD56^+CD3^-$), neutrophils ($CD15^+$), monocytes/macrophages ($CD14^+$), and $CD45^-$ non-hematopoietic cells isolated from HCC tumors (n=6). **(E)** Gating strategy for FACS sorting. $PD\text{-}L1^-$ and $PD\text{-}L1^+$ subsets were sorted according to patterns of PD-L1 expression. **(F)** Expression of key glycolytic enzymes gene in $PD\text{-}L1^+$ and $PD\text{-}L1^-$ macrophages purified from human HCC tumors (n=3).

Figure S2

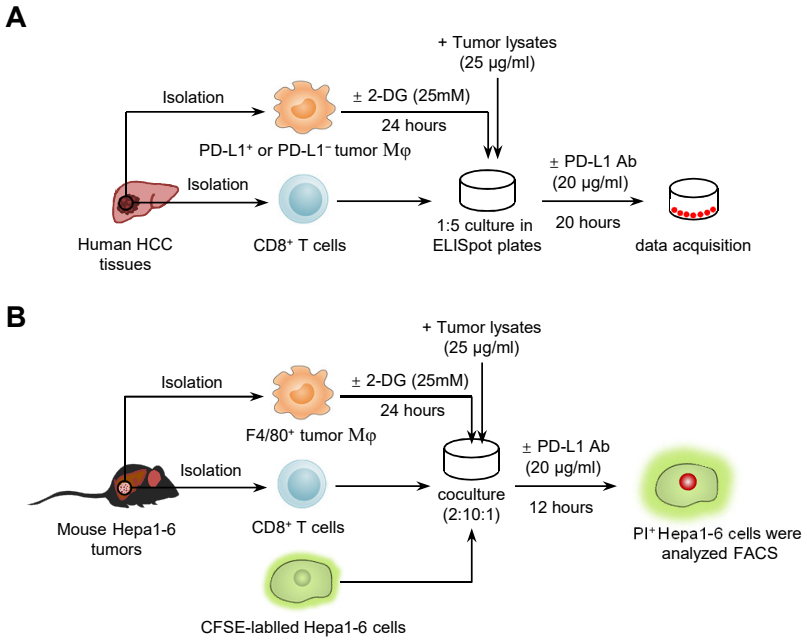

Figure S2. The effect of PD-L1 blockade and glycolysis inhibition on tumor macrophages -elicited cytotoxic T cell function. (**A**) Schematic procedures for Figure 2A. IFN-γ detection by ELISpot in HCC tumor-derived T cells cultured alone or with PD-L1^{-} or PD-L1^{+} macrophages (Mφ), or with those cells pre-treated with 2-DG, anti-PD-L1 antibody, or IgG1 (n=5). (**B**) Schematic procedures for Figure 2B. Cytotoxic effects of tumor T cells on CFSE-labelled autologous mouse Hepa1-6 hepatoma cells in the presence or absence of tumor Mφ that were left untreated or pre-treated with 2-DG, anti-PD-L1 antibody, or IgG1 (n=6). Propidium iodide^{+} apoptotic tumor cells were measured by FACS.

Figure S3

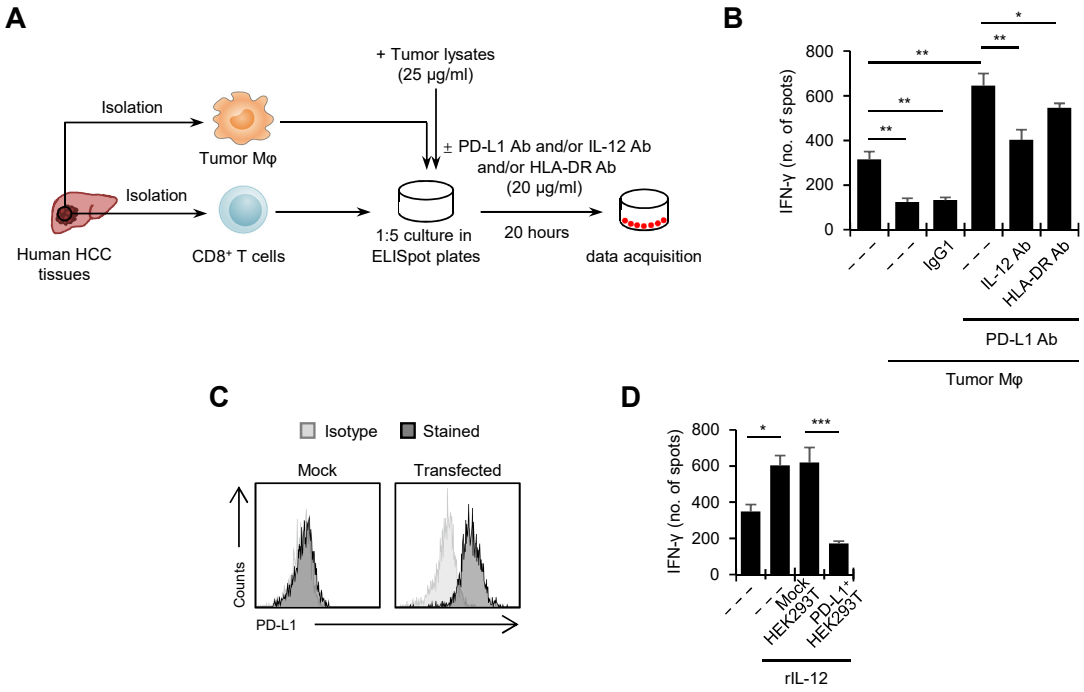

Figure S3. The effect of IL-12 or HLA-DR on tumor macrophages-elicited cytotoxic T cell function upon PD-L1 blockade. (A and B) Macrophages (Mφ) from human HCC tumors were cultured with autologous tumor-derived $CD8^+$ T cells for 20 hours in the presence or absence of an anti-PD-L1 antibody, and/or anti-IL-12 antibody, and/or anti-HLA-DR antibody. Meanwhile, 25 μg/ml of tumor mass lysates were added to trigger tumor specific T cell response **(A)**. IFN-γ production in $CD8^+$ T cells was analyzed by ELISpot **(B)**. **(C)** Efficiency of PD-L1 over-expression in Huh7 cells (n=3). **(D)** IFN-γ detection by ELISpot in HCC tumor-derived T cells cultured alone or with Mock or PD-L1 HEK293T transfectants in the presence or absence human recombinant IL-12 antibody (n=5). Results represent mean ± SEM of four independent experiments (n=5). *P<0.05, **P<0.01, ***P<0.001, one-way ANOVA followed by Bonferroni's correction.

Figure S4

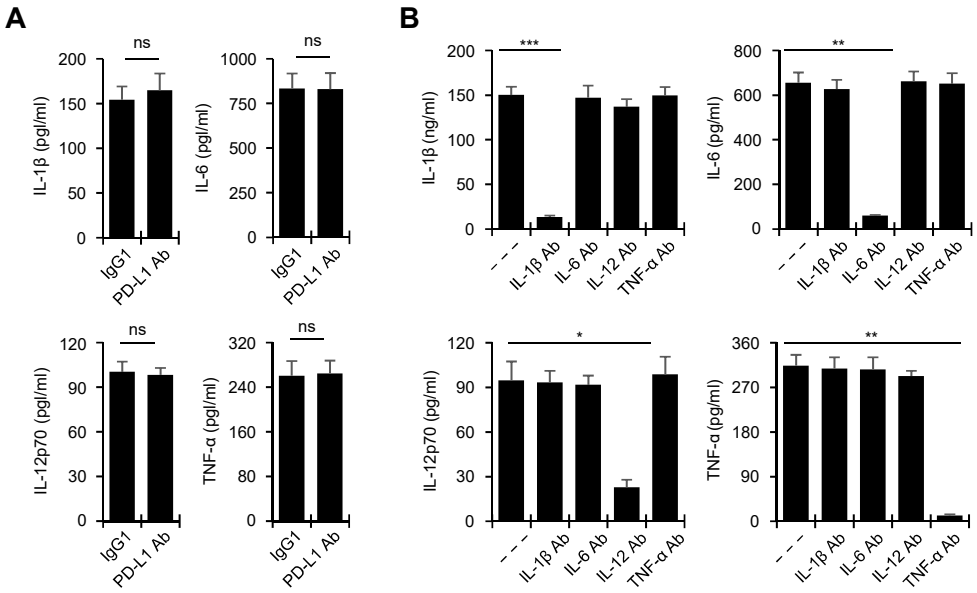

Figure S4. Blocking the PD-L1 in PD-L1^{+} macrophages did not affect the production of proinflammatory cytokines. (A) Effects of PD-L1 blocking antibody on proinflammatory cytokines expression in macrophages isolated from human HCC tumors (n=4). **(B)** Macrophages from human HCC tumors were treated with indicated neutralizing antibodies or isotype IgG for 24 hours. IL-1β, IL-6, IL-12, and TNF-α production were determined by ELISA (n=5). Results represent mean ± SEM of four independent experiments. *P<0.05, **P<0.01, ***P<0.001, one-way ANOVA followed by Bonferroni's correction.

Figure S5

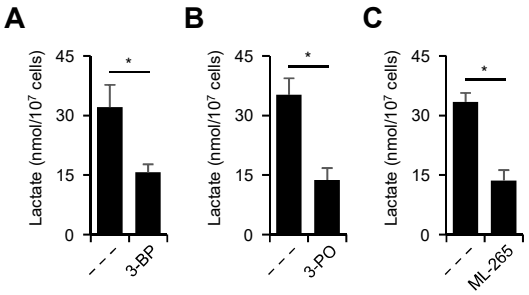

Figure S5. Effects of key glycolytic inhibitors on lactate production. (A-C) $CD14^+$ cells purified from peripheral blood of HCC patients were treated with supernatant from primary HCC cells (HCC-SN) in the absence or presence of 3-BP **(A)**, 3-PO **(B)**, or ML-265 **(C)** for 24 hours (n=7). Lactate production was measured with a lactate assay kit. Results represent mean ± SEM of four independent experiments. *P<0.05, Student's t-test.

Figure S6

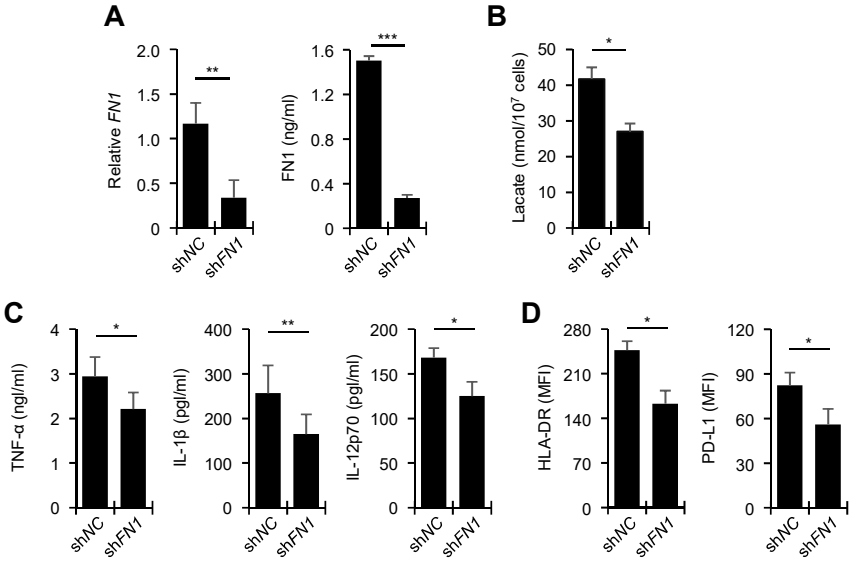

Figure S6. FN1-knockdown cells showed impaired ability to induce PD-L1 expression in monocytes. (A-D) Knock-down of *FN1* **(A)** in Huh7 cells suppressed lactate production **(B)**, inflammatory cytokine expression **(C)**, as well as HLA-DR and PD-L1 expression **(D)**, in Huh7 culture supernatants treated monocytes (each n=4). Results are expressed as the mean ± SEM. *P<0.05, **P<0.01, ***P<0.001.